The application of spatial derivatives to non-potential field data interpretation

David Beamish

British Geological Survey, Keyworth, Nottingham, NG12 5GG, UK.

Geophysical Prospecting, 2012, **60**, 337-360.

David Beamish

British Geological Survey, Keyworth, Nottingham, NG12 5GG, UK

Email: dbe@bgs.ac.uk.

Tel: +44(0)115 936 3432

Fax: +44(0)115 936 3261

Keywords:

Airborne geophysics, Data processing, Electromagnetics, Magnetics, Potential Field, Resistivity

Abstract

Source/body edge detection is a common feature in the processing and interpretation of potential field data sets. A wide range of spatial derivatives are available to enhance the information contained in the basic data. Here the ability of these procedures to assist with the mapping interpretation of non-potential field data is considered. The study uses airborne electromagnetic (conductivity) data but also provides a general context for other conductivity/resistivity data, provided the non-potential field nature of active, and thus spatially-focused, measurements is acknowledged. The study discusses and demonstrates the application of a range of common spatial derivative procedures, including the analytic signal and upward continuation, to both magnetic and conductivity data. The ability of the tilt derivative to provide enhanced mapping of conductivity data is considered in detail. Tilt and its associated functions are formed by taking combinations of vertical and horizontal derivatives of the data set. Theoretical forward modeling studies are first carried out to assess the performance of the tilt derivative in relation to the detection and definition of concealed conductivity structure. The tilt derivative embodies Automatic Gain Control that normalizes the detection and definition of both weak and strong conductivity gradients across an appropriate subsurface depth range. The use of high order spatial derivatives inevitably results in a degree of noise (cultural perturbation) amplification that is survey and technique specific. Both of these aspects are considered using practical case studies of jointly obtained magnetic and conductivity data at a variety of spatial scales.

1. Introduction

Magnetic and gravity derivatives have a well-established role in the interpretation of potential field data from both ground-based and airborne surveys. A range of processing procedures and filters exist, largely based on vertical and horizontal derivatives and their combinations that perform as enhanced mapping functions when applied to the basic data sets (Blakely 1995; Cooper and Cowan 2006). The source parameters that are typically estimated are the boundaries or edges of *singular* source bodies (Blakely and Simpson 1986; Cooper and Cowan 2008). The complications arising in the case of multiple bodies are then typically studied as a form of interference of the simple case (e.g. Salem *et al*. 2007). In addition to these mapping functions, other methods such as Euler deconvolution (Thompson 1982; Reid *et al*. 1990; Li 2003) also exist for the estimation of the depth of the source. In the present study only established mapping capabilities and their extension to assist with the interpretation of non-potential field data are considered. One particular technique, the tilt derivative (Millar and Singh 1994) that has been used as an enhanced edge detector is considered in detail.

A number of case studies and theoretical assessments are presented using airborne electromagnetic (AEM) frequency domain, data acquired alongside magnetic data. Electromagnetic (EM) data acquired by airborne frequency domain systems comprise coupling ratios of secondary to primary field ratios at individual frequencies (e.g. Fraser 1978). These data exhibit a sensitive dependence on altitude. Spatial gradients exist in these data due to inherent variations in flying altitude. These primary data are therefore not suitable for an analysis based on their spatial gradients. The standard method of removing the altitude dependence is to convert the coupling ratios to estimates of apparent, half-space resistivity, at each frequency. The most common procedure employs the Fraser pseudo-layer transform (Fraser 1978). Inversion procedures may also be used to estimate the half-space resistivity (Beamish 2002, 2004a). Such estimates provide conductivity models with a validity that depends on a vertically uniform, 1D assumption. It should also be noted that different airborne systems (including frequency and time domain systems together with their specific bandwidths) will provide different EM interactions with specific 3D targets. It is the detection and definition of the lateral gradients generated by non-1D conductivity structure that forms the basis of this study. Although this study considers AEM survey data, the concept can equally well be applied to ground-based conductivity/resistivity data sets.

The use of spatial gradients in the interpretation of conductivity or resistivity data sets is not established to the same degree as those associated with potential field data. Beamish (2004a) previously discussed the use of sun-shade (shaded-relief) and horizontal derivatives in relation to the mapping and delineation of 3D conductivity variations. The responses from different frequency domain airborne systems were considered. Compact 3D bodies give rise to dipolar horizontal derivative responses. The field interactions involved in EM induction within a 3D conductivity contrast are profoundly more complex than the potential field generated in an equivalent magnetic susceptibility/density case. It is known that in the limit of low frequency and very high contrast targets, the EM wave equation may approximate Laplace's equation (Roy 1966). This condition was discussed by Cooper, Combrinck and Cowan (2004) who went on to consider the application of Euler deconvolution to airborne time-domain data. The more general inductive case is considered here and the studies are based on conductivity information derived from airborne frequency-domain electromagnetic data.

The processing algorithms applied to potential field data sets are highly developed and well-established in the literature (Nabighian *et al.* 2005). The potential fields, satisfying Laplace's equation, contain the superposition of the effects of all subsurface bodies. The non-potential fields considered here are provided by active measurements which operate across a specific local scale (a subsurface volume) that can be defined for any particular ground or airborne electromagnetic or electrical method. Thus the AEM measurements considered here are primarily sensitive to material content within a quite compact scale, typically less than 100 m in all 3 dimensions. A number of potential field processing procedures, such as vertical continuation, may be considered appropriate only for potential fields. This arises since existing potential field theory allows the transformed results to be used as a basis for modeling. As long as it is recognized that the same transformed non-potential field data cannot be 'treated' in the same manner then the inherent filtering aspect of the transformation can still be successfully applied to non-potential field data.

These general concepts are first introduced and then demonstrated on a 20 x 20 km test area of data taken from a large airborne geophysical survey of Northern Ireland (named Tellus). The magnetic and half-space conductivity data are used to illustrate the application of shaded-relief, the analytic signal, upward continuation and the tilt derivative to both data sets. The tilt derivative (TDR) embodies Automatic Gain Control (AGC) that normalizes the detection and definition of both weak and strong geophysical gradients across an appropriate subsurface depth range. In the magnetic case, the depth scale of detection may only be limited by survey scale (and inherent signal/noise characteristics). In the electromagnetic case the depth scale of detection is largely related to frequency with the lowest frequency providing the largest depth of investigation. Deeper features tend to provide the lowest signal/noise gradients within a geophysical data set and it is the ability of the TDR response to define such features that potentially provides an enhanced mapping capability.

A range of forward modeling studies of the magnetic TDR response have been presented in the literature. Here, theoretical electromagnetic forward modeling studies are carried out to assess the performance of the tilt derivative in relation to the detection and definition of concealed conductivity structure. Both thin-sheet, compact prismatic bodies and a faulted half-space are considered across a depth range from the near surface to a depth of 150 m. In contrast to the magnetic case, conductivity data are one-sided (positive) and the mapping of the TDR conductivity response to provide equivalent functionality is demonstrated to be a simple 45º shift. Although the magnetic tilt derivative may be used to estimate depth to source, the more complex field interactions involved in the electromagnetic case preclude this option.

The use of the spatial derivatives embodied in the TDR response results in a degree of noise amplification that is survey and technique specific. Airborne geophysical data sets, particularly those collected at low elevations, are subject to a range of cultural perturbations. Here, the artificial features of both magnetic and conductivity data sets are retained to demonstrate the range of spatial wavenumbers acquired by modern UK airborne geophysical surveys and to illustrate their influence on the processing procedures considered here.

The tilt derivative may be applied to any scale of resistivity or conductivity data, either in profile or gridded form. It has been found to be particularly useful when applied to large scale data sets in relation to mapping the spatial attitude and coherence of regional scale features. The results for the whole Northern Ireland magnetic and conductivity data sets are presented, compared and discussed. This is followed by a final, detailed case study that allows the performance of the conductivity TDR to be assessed at the local (< 200 m) scale.

2. Background Concepts

The processing and detection algorithms applied to potential field data sets are highly developed and well-established. It is not generally appreciated that the procedures can also be usefully applied to other non-potential field geophysical data sets. The physical basis and thus subsequent interpretation of the results of applying such

algorithms to non-potential field data is, however, necessarily a distinct case that requires further consideration. We here consider the particular case of applying spatial derivatives to gridded conductivity/resistivity data sets in relation to the existing knowledge that pertains in the case of potential field data. The application of spatial derivatives, often called data transformation, is well described in the potential field case by Blakely (1995). Although the techniques are now often incorporated into procedures for subsurface depth estimation of causative bodies, we here restrict the majority of the discussion to the mapping of lateral information (i.e. the detection of structural/body edges).

Potential field data measured in geophysical investigations contain the superposition of the effects of all subsurface sources. Local information, from shallow sources, for example, is often superimposed on a regional field that comes from larger or deeper sources. The estimation and subtraction of a regional field can provide a residual field that better defines the shallow features. The processing of potential data to provide enhanced mapping capabilities is well-established and uses a suite of routine spatial transformation/filtering operations that are typically based on the Fourier components of the data spectrum. Thus potential field data sets may be subjected to procedures to enhance their higher wavenumber content such as high-pass filters, downward continuation and the estimation of vertical and horizontal derivatives. Other procedures routinely used to enhance longer wavelengths include low-pass filters, upward continuation and integration.

A number of the procedures, including that of vertical (upward and downward) continuation and vertical derivative calculations are often considered useful only to potential fields since they have an established basis in terms of existing potential field theory (Blakely 1995). Thus, when considering potential fields, the fields obtained by vertical continuation can be considered transformed observations that can be modelled by a given source distribution. The same will not apply to non-potential field data. Nevertheless, as is demonstrated later, the filtering operation involved in the procedure is of general use.

The primary difference between the information content of a potential field and a non-potential field (e.g. electromagnetic or electrical) ‘active’ measurement lies in the spatial wavenumber content of the information. It should also be noted that the non-potential information discussed here is the *secondary* conductivity/resistivity information derived from the *primary* geophysical fields involved in the measurement (e.g. electromagnetic coupling ratios and voltage and current in the case of DC resistivity measurements). The active measurements are in fact focused within a definable subsurface volume and each individual measurement relates to a localised spatial scale. In the case of the AEM data considered here, the lateral spatial scale of the information obtained is usually defined by a footprint (Liu and Becker 1990; Kovacs Holladay and Bergeron 1995).

The full volumetric spatial scale of an AEM measurement can be either defined in terms of a geometrical (non-plane wave) skin depth (Beamish 2004b) or by considering a volumetric sensitivity function (McGillivray *et al.* 1994; Suppala *et al.* 2005; Tølbøll and Christensen 2007). The vertical and horizontal distances involved the AEM measurement are geometrically complex (Beamish 2004b) and depend on

frequency, subsurbsurface conductivity and altitude. For the survey considered here, each measurement may typically be associated across a principal area of sensitivity of less than 100 x 100 m over the ground surface. The depth of investigation depends on frequency and the vertical distribution in conductivity. At the lower frequencies (912 and 3125 Hz) considered here a principal sensitivity to conductivity variations in the upper 60 m is achieved; this may extend to depths in excess of 100 m in appropriate resistive terrain.

3. The test data sets

In order to provide a framework for the study conducted here, magnetic and electromagnetic (conductivity) data obtained from an airborne geophysical survey of Northern Ireland are used (Figure 1). Following a description of the whole data set, the magnetic and conductivity information obtained across a 20 x 20 km study area are first introduced and described.

3.1 The Tellus airborne geophysical survey of Northern Ireland

The Tellus airborne survey of Northern Ireland was conducted over a two year period (2005 and 2006) and acquired magnetic, radiometric and electromagnetic geophysical data (Beamish and Young 2009). Flight lines were spaced at 200 m intervals and oriented at 345º, on the basis of geological trends. The nominal flight height was 56 m, rising to 200 m over populated areas. The survey acquired over 81,000 line-km of data. The magnetic data were acquired with a wing-tip mounted Cs vapour magnetometer with an along-line sampling of ~ 6 m. The frequency domain electromagnetic system is described by Leväniemi *et al.* (2009) and comprises pairs of vertical coplanar, wing-tip sensors. The two frequency EM system used in 2005 (3125 and 14368 Hz) was replaced by a new four frequency system during 2006 (912, 3005, 11962 and 24510 Hz). At the typical flying speed of ~60 m/s, along-line sampling of the electromagnetic data is ~15 m.

3.2 The test data

We first consider a 20 x 20 km study area taken from the Tellus airborne geophysical survey of Northern Ireland as described above. The selected area is shown on the location map of Figure 1. The geophysical data are shown in relation to the 1:250k geological map, with the addition of fault lines, in Figure 2. All three images in Figure 2 are shown using the same 3D perspective view to emphasise the wavenumber content and dynamic range of the geophysical data. The data were both gridded using a 50 x 50 m grid cell size. The Total Magnetic Intensity (TMI) anomaly data, reduced-to-pole, were gridded using a bi-directional gridding algorithm while the conductivity data were gridded using a natural-neighbour algorithm to preserve their strong edge-content.

Figure 2a shows the 1:250k geological map centred on the Lack Inlier (purple) within a Carboniferous basin setting. The Dalradian Inlier comprises metasedimentary and

ultrabasic rocks with high susceptibility and high density. The inlier is bounded by the Cool Fault (CF) to the north and by the Omagh Thrust Fault (OT) in the south. The geological setting and tectonic framework of the area is described in Mitchell (2004). The population centres of Omagh and Castlederg are indicated by cross-hature along the edges of Figure 2a. At the scale shown, 4 igneous intrusions (dykes, D) are shown trending in a discontinuous manner NW-SE across the area. The strikes are oblique to the other prevailing structural trends.

The TMI data and the electrical conductivity data for the area are shown in Figures 2b and 2c, respectively. For the analysis conducted here, data sets that retain cultural perturbations are used. Although complete or partially decultured data can be generated to provide more robust geological interpretations, the artificial features of both the data sets are retained to demonstrate the wide-range of spatial wavenumbers acquired by modern UK airborne geophysical surveys and to illustrate their influence on the processing procedures considered here. The TMI data presented here are reduced-to-pole and both geophysical images shown in Figures 2b and 2c use a linear colour scale.

The TMI data shown in Figure 2b display a long wavelength positive zone showing a high degree of correlation with the Lack Inlier. Within this broad zone, a series of positively-enhanced features are superimposed representing more detailed structural information contained within the inlier. In the NW corner of the image an isolated, northerly trending zone of high amplitude positive anomalies is observed. Across the data set, a series of relatively low amplitude and largely isolated positive features are observed; these are the magnetic responses due to cultural artefacts such as farm-buildings. One of the larger cultural perturbation features, identified from detailed topographic maps (Lahti *et al.* 2007), is labelled C in Figures 2b and 2c.

The main negative TMI data excursions are associated with a series of reversed polarity dyke structures which traverse the area with a predominant NW-SE trend. These are interpreted as components of the larger Palaeogene Donegal-Kingscourt dyke swarm (Chacksfield 2010). In detail, the TMI data resolve considerable complexity in terms of terminations and localised deviations of these dykes across the area. In addition a few positively magnetised dyke-like structures, again with a NW-SE trend, are observed to the north of Cool Fault/Lack Inlier.

The conductivity image, obtained at a frequency of 3125 Hz, shown in Figure 2c displays a greater association with the bedrock geology than the mapping provided by the TMI data; conductivity gradients are associated with the general outline of the Lack Inlier and with the northern limit of the Carboniferous outcrop (northern-most grey polygon, Fig. 2a). Both the Cool Fault and eastern section of the Omagh Thrust Fault exhibit localised and high amplitude conductivities that are likely to be associated with tectonic mineralisation episodes. The conductivity data may track mineralisation associated with fluid (brine) flow events in the late Caledonian as described by Parnell *et al.* (2000). Non-geological perturbations also exist in the conductivity data set. Some perturbations are isolated, such as the feature labelled C, but others of lower amplitude are quasi-linear features associated with road edges and their concomitant service routes (assumed).

As discussed previously, although the conductivity information is associated with a localised and focused measurement, longer wavelength information is also contained in the assembled conductivity image by virtue of the spatial persistence of conductivity amplitudes such as those associated with bedrock geology. In order to discuss wavelength contributions further, radial/azimuthal averaged (2D) power-spectra were calculated using the geophysical grids presented in Figure 2. The lowest wavenumber is determined by the number of cells within the grids i.e. the scale length of the data. Here the grid size is 20 x 20 km, so that the limiting wavelength approaches 10,000 m. The shortest wavelength represents the Nyquist sampling interval which, in this case, is 100 m. The power spectra obtained are shown in Figure 3 (lines with no symbols). When the spectra for the TMI and conductivity grids are compared in their 'natural' units (TMI anomaly data in nT and conductivity data in mS/m) it is found that the power levels of the TMI data exceed those of the conductivity data. Both spectra are 'red' and power levels at the longest wavelengths dominate. Over the wavelength interval from 100 to 1000 m, the two spectra display approximately parallel increasing behaviour but at wavelengths greater than 1000 m the rate of increase in power level is reduced in the conductivity spectra. In broad terms, the spectral content of the two data sets is broadly similar despite the very different nature of the two geophysical data sets.

4. Spatial derivatives of the test data

The spatial derivatives of a measured quantity T comprise two horizontal derivatives ($\partial T/\partial x$ and $\partial T/\partial y$) together with a vertical derivative $\partial T/\partial z$. Blakely (1995) discusses the calculation of the 3 gradient terms from the point of view of a smoothly varying scalar quantity measured on a horizontal surface. It is noted that the horizontal derivatives (the first 2 terms) are easily estimated using simple finite-difference methods applied to discrete measurements of the quantity T. If the quantity T is a potential, then Blakely (1995) notes that we can also calculate vertical gradients from the horizontal derivatives. A 3-stage procedure, involving Fourier transformation of the data, multiplication by the appropriate wavenumber term, and inverse Fourier transformation of the product is described. This procedure is now a standard method used in both filtering operations and in the calculation of derivative terms of potential field data.

Given the x component wavenumber k_x and the y component wavenumber k_y, the vertical derivative, of a potential function, is calculated by multiplication of the spectrum by $|k_z|$ where:

$$k_z = \sqrt{(k_x)^2 + (k_y)^2} \quad \text{.....(1)}$$

It should be evident that for the scalar data considered here (including non-potential field data) the horizontal derivatives exist and are meaningful in the sense that they form a measure of the rate of change of the quantity in the two horizontal directions. Given the existence of these two quantities, an estimate of the vertical gradient is then obtained using equation (1). In the case of potential fields, the vertical derivative has a specific mathematical relationship with the causative source body. In the case of non-

potential field data, we are considering a quantity (a physical property) and not a field and no such simple association is possible. Nevertheless, as noted by Blakely (1995), the spectral multiplication by k_z in equation (1) clearly enhances the high wavenumber components in the data and can be seen to constitute a filtering operation. In detail the vertical derivative calculated according to equation (1) is an estimate since it is based on a number of underlying premises such as that of a horizontal plane of measurements. Its use in calculations based on harmonic and non-harmonic functions is further discussed by Florio *et al.* (2006).

The first and second vertical derivatives (e.g. Blakely 1995) are used as general mapping procedures since they accentuate and help to resolve the edges of short wavelength sources. The presentation of such information is not routinely accompanied by any mathematical interrogation. The principle aim is to aid interpretation. In a similar manner, the observed and theoretical case studies considered here are intended to illustrate that all 3 spatial derivatives can provide useful mapping procedures to accentuate or attenuate specific features of the spatial gradients .

Three procedures that are routinely used in the processing of potential field data are now applied to both example data sets in order to illustrate the application of potential field methods to conductivity data. A fourth procedure, the application of the tilt derivative, is first described and later assessed following a theoretical modelling study of its application to electromagnetic data.

4.1 Shaded-relief

The first method considered is the shaded-relief (or sun-shade) algorithm. The application of shaded-relief is a commonly used technique for emphasising features in an image that have a specific orientation. The procedure that forms the reflectance image involves the use of two orthogonal horizontal gradients (Horn 1982). Beamish (2004a) previously discussed the use of sun-shade and horizontal derivatives in relation to the mapping of lateral gradients due to 3D conductivity variations.

Although there may be a wide variety of implementations of the procedure, there are typically 3 main parameters that require to be specified including horizontal (declination) and vertical (inclination) of the illumination source and a scale factor (sometimes called a vertical exaggeration) controlling the degree of shade applied. For data sets containing a variety of strike azimuths, at least two horizontal angles are usually considered. A shaded-relief algorithm applied to the conductivity and TMI data sets provided the continuous grayscale images shown in Figures 4a,b (conductivity) and Figures 4c,d (TMI) for the two orthogonal horizontal sun azimuths of 135° and 45º (indicated by arrows). All images use a vertical sun angle of 45º and the same illumination contrast scale factor is applied throughout. As can be seen in Figure 4, the algorithm attenuates the longer wavelength information and emphasizes the gradients due to shorter wavelength features in the data.

The conductivity images (Figure 4a,b) are dominated by the high amplitude conductivity zones associated with the Cool Fault and Omagh Thrust Fault (Figure 2a). The amplitudes are sufficiently large to ensure a high level of discrimination at both azimuths. Elsewhere a series of high-wavenumber, quasi-linear gradients are observed many of which are road responses but some of which are geological (e.g. those within the Lack Inlier). The road associations are obtained using detailed topographic maps at much smaller scales than the information discussed here. Within the images of Figure 4a,b it also possible to detect a longer wavelength perturbation associated with the northern edge of the Carboniferous outcrop, noted previously.

Resolution of the pervasive dyke structures in the TMI images (Figure 4c,d) is a strong function of the horizontal azimuth of the sun angle and an additional sun-angle is also required to fully evaluate the continuity of oblique features, particularly within the Lack Inlier. Also apparent throughout both images are the large number of isolated, high-wavenumber artefacts due to magnetic cultural perturbations.

4.2 Analytic signal

Nabighian (1972) discussed the analytic signal of magnetic anomalies arising from 2D sources. An important characteristic of the analytical signal is that is independent of the direction of the magnetization of the source. The amplitude of the analytical signal is also related to the amplitude of magnetization.

Here the 3D analytic signal amplitude (Roest Verhoef and Pilkington 1992) is calculated from the gridded data shown in Figure 2. The analytic signal amplitude (ASA) when applied to gridded observations of a field (T) is defined as:

$$ASA = \sqrt{\left(\frac{\partial T}{\partial x}\right)^2 + \left(\frac{\partial T}{\partial y}\right)^2 + \left(\frac{\partial T}{\partial z}\right)^2} \quad \text{.....(2)}$$

The ASA, or total gradient, is thus defined by derivatives in all 3 dimensions and is sensitive to high-order wavenumber gradients in the data. The analytic signal amplitudes for both the TMI and conductivity grids are shown as contoured plots in Figures 5a and 5b, respectively. The ASA for the TMI data (Figure 5a) range from 0.001 to 8.9 nT/m and the data are contoured using a linear interval of 0.1 nT/m. Contour lines are coloured with lighter colours representing increasing contour values. The ASA for the conductivity data (Figure 5b) range from 0.0001to 11.3 mS/m^2 and the data are contoured using a linear interval of 0.1 mS/m^2.

The results shown in Figure 5 demonstrate a clear correspondence with the gradients detected by the shaded relief information of Figure 4. One advantage of the ASA processing is that the information is now independent of the three sun-shade parameters and it provides a numerical assessment of the total gradients in the data. A clear disadvantage is that the more subtle spatial continuity of gradient information provided by the shaded relief image is lost. The ASA of the TMI data has a potential role to play in the identification of many of the isolated instances of cultural perturbations seen in Figure 5a. In a similar manner the ASA applied to the

conductivity data allows the largest cultural perturbations (gradients) to be identified and potentially removed from the data set.

4.3 Upward Continuation

The procedure of upward continuation is a specific form of wavelength filtering and is essentially used to calculate the potential field of a data set at an altitude greater than that of the measured height. As noted by Blakely (1995), the basis for the procedure lies in the fact that a potential field can be calculated at any point within a region from the behaviour of the field on a surface enclosing the region. In the case of potential fields, the procedure is rigorous for data collected at a uniform height, thus allowing modelling procedures, for example, to use the upward-continued field. This, of course, will only apply in the specific case of potential fields.

In the Fourier domain, upward continuation is achieved by a simple exponential transform (Blakely 1995, equation 12.8) that reduces the high wavenumber content of the data set and also reduces spatial resolution. The procedure operates by Fourier transforming the measured data, multiplying by the exponential transform and then inverse Fourier transforming the product. The transform is a specific form of low-pass filtering operation. The exponential transform is considered a 'clean' form of filtering since it produces almost no side effects. Such a filtering operation, along with all other forms of low-pass, high-pass and band-pass filters can be applied to any data set.

In geophysical processing it is common to upward continue potential field grids in multiples of the grid cell size. The amount of upward continuation is governed by the wavenumber content of the data set and the desired outcome in terms of attenuation of high wavenumber components. Here an upward continuation distance of 100 m (a distance of two grid cell sizes) has been applied to demonstrate the procedure. It should be noted that the amount of upward continuation is not necessarily optimised to the interpretation of the two data sets. The 2D power-spectra of the upward continued grids are shown in relation to the unfiltered grids in Figure 3. The progressive attenuation of the power levels with increasing wavenumber in both data sets is very evident. At the Nyquist wavenumber, the transform provides power level attenuation of 9 orders of magnitude in the TMI data set and 12 orders of magnitude in the conductivity data set. At a wavelength of 1000 m, the attenuation has reduced to 1 to 2 orders of magnitude in both data sets.

To further illustrate the effect of the filter on the two data sets, the ASA of the upward continued data was calculated and is shown, in relation to the results discussed previously, in Figures 5c,d. The maximum values of the upward continued data are considerably reduced. The ASA for the magnetic data (Figure 5c) now range from 0.0003 to 1.62 nT/m and the data are again contoured using a linear interval of 0.1 nT/m. The ASA for the conductivity data (Figure 5d) range from 0.00009 to 1.2 mS/m^2 and the data are contoured using a linear interval of 0.1 mS/m^2. The broad effect of the upward continuation can be seen to be a either a removal or significant attenuation of the high wavenumber gradients in the original data. Such gradients may be either geological or cultural. The wavenumber content remaining in both data sets

is naturally highly modified however the discussion and examples serve to demonstrate the applicability of upward continuation to non-potential field data.

4.4 The Tilt Derivative

The tilt angle or derivative (TDR) is defined by Millar and Singh (1994) as the arctangent of the ratio of a vertical to a combined horizontal derivative:

$$TDR = \tan^{-1}\left[\frac{\partial f / \partial z}{\sqrt{(\partial f / \partial x)^2 + (\partial f / \partial y)^2}}\right] \qquad (3)$$

where f is the magnetic or gravity field. More recently, Verduzco *et al*004) suggested using the total horizontal derivative (THDR) of the tilt angle, as an improved edge detector:

$$THDR = \sqrt{(\partial F / \partial x)^2 + (\partial F / \partial y)^2} \qquad (4)$$

where F = TDR. The amplitude range of the dimensionless ratio TDR is restricted to the range $\pi/2$ to - $\pi/2$ (or 90° to -90°) by virtue of the arctan function. The TDR acts as an Automatic Gain Control (AGC) filter when applied to the field observations. This is an important feature when considering its application to larger scale data sets with a wide dynamic range. It is possible to consider additional functions that may be derived from tilt using higher order derivatives such as the total horizontal derivative of the TDR (equation 4). However, as noted by Cooper and Cowan (2006), as the order of the derivative function increases, in the search for higher resolution, the degree of noise amplification also increases. The signal/noise content of the data considered is thus an important aspect in relation to the practical application of the procedures. In general for UK onshore, low level airborne data, with their inherent cultural perturbations, the use of higher order derivatives can be problematic.

Theoretical studies of the TDR applied to magnetic models are presented by Fairhead *et al.* (2004), Verduzco *et al.* (2004), Cooper and Cowan (2006), Salem *et al.* (2007) and Salem *et al.* (2008). The majority of the magnetic modeling studies consider the TDR response of simple isolated bodies since the principal objective is to provide procedures that delineate the vertical edges of concealed magnetic structures. Salem *et al.* (2007) also noted that in addition to edge detection, the TDR method can also provide an estimate of the depth to the source body (in the case of simple bodies) using the distance between the zero contour and either the -45º or +45º contours of the TDR response. The magnetic modeling presented by Salem *et al.* (2007) relates to simple magnetic bodies with vertical contacts and with vertical magnetization vectors (a magnetic inclination of 90º). Such bodies give rise to a TDR response that approaches +90º above the magnetic body and -90º some distance away from the body. As noted by Beamish and White (2011) if the magnetization vector is reversed, the TDR response is inverted. The contour mapping of the TDR response to identify and outline magnetic sources would typically involve the intervals from -45º to 0º,

from 0º to +45º and from 45º to +90º. The zero contour would identify the edge location with the interval above zero defining the area underlain by the source. As noted by Verduzco *et al.* (2004), varying angles of magnetic inclination will also modify the behavior of the TDR response as will dipping structures (Lahti and Karinen 2010). A theoretical evaluation of the TDR procedure applied to simple models of conductivity structure is now presented.

5. Synthetic modelling studies of the TDR response applied to conductivity data

As discussed above, when the tilt derivative is derived from non potential field data, the function in equation (3) may be replaced by resistivity or conductivity. In order to evaluate the performance of tilt derivatives in relation to conductivity data we consider the airborne EM system used on the Tellus survey of Northern Ireland and discussed previously. The system provides data at four frequencies that relate to depths of investigation that increase with decreasing frequency. In principal the TDR procedure may be applied to each of the half-space conductivity distributions and thus structural contributions across different depth scales may be assessed. The lowest frequency is 912 Hz and this provides the greatest depth of investigation.

It should be noted that in the absence of conductivity gradients/structure no lateral gradients in the EM data, and derived conductivity distribution, are produced. The forward modeling studies consider 2D/3D bodies that provide lateral gradients that are assessed using the TDR response. The transformation/inversion of the EM data to an apparent half-space conductivity is based on the 1D assumption which will be incorrect at locations (e.g. near body edges) where gradients are produced. The procedure, however, is that applied to field observations to generate apparent conductivity data sets and the results obtained by the modeling are therefore consistent with the procedures applied to observational data.

5.1 Thin-plates

3D EM modeling of thin-plate conductivity structures offers the simplest and, typically, the most stable set of solutions for the forward EM modeling case. Here the thin-plate modeling algorithm LeroiAir developed by the CSIRO Electromagnetic Modeling Group is used for the computations. The method is based on the work of Weidelt (1981). A single vertical thin-plate with a depth extent (in z) of 100 m and a length (in y) of 1.5 km was embedded in a uniform host of 5 mS/m. The conductance of the plate was set at 10 S (e.g. a 10 m thick sheet with a conductivity of 1 S/m) and the survey height was set at 50 m. Survey profiles (flight lines) were defined in the x-direction, perpendicular to the plate. By using a large plate length, it is possible to generate profiles and grids over the central area of the model (e.g. 200 x 200 m) free from the 3D edge effects of a more compact body. Computations were performed with the upper surface of the plate increasing from the near-surface to a depth of 150 m. The coupling ratios calculated from the forward modeling at 912 Hz were then converted to half-space apparent conductivities in the standard manner. Figure 6a shows the apparent conductivity results obtained across a profile through the centre of

the model with the vertical plate located below the origin. The detection amplitudes (i.e. subtracting the background conductivity of 5 mS/m) of the plate decrease with increasing depth and range from 40 mS/m at the shallowest depth to 1.5 mS/m with the plate at a depth of 150 m. The TDR response of these data is shown in Figure 6b. As the plate increases in depth to 150 m, the assessment of the target location increases to a width of some +/- 45 m. The infilled region of the TDR response indicates how mapping of the TDR response across two intervals from 0º to 45º and 45º to 90º would characterize the location of the thin (vertical) conductive zone.

The total horizontal derivative (THDR, equation 4) of the tilt angle is shown in Figure 6c for the two limiting plate depths of 25 and 150 m. The broad wavelength of the THDR response increases with increasing depth of the target and a local minimum (theoretically a zero) is necessarily observed across the central maximum of the TDR response. In the case of real data, both responses amplify noise and this has been found to be excessive in the case of the THDR method. Generally, the simpler form of the TDR response is preferred.

5.2 Elongated 3D prisms

A second class of models that have been studied comprise 3D prisms of finite extent. Again by using a large prism length, it is possible to generate profiles and grids over the central area that approximate elongate 2D structures. 3D forward modeling in the case of prisms was carried out using the EMIGMA™ modeling package (Habashy Groom and Spies 1993).

The model considered here comprises two conductive prisms with cross-sectional dimensions (in x and z) of 100 x 50 m. The length of each prism (in y) is 2 km. The upper surface of the first prism (A) is at a depth of 50 m while that of the second prism (B) is at 150 m. The conductivity of each prism is set at 100 mS/m and the prisms are embedded in a uniform background of 2 mS/m. Forward modeling of the airborne response was undertaken assuming a survey altitude of 50 m. Survey profiles (flight lines) were defined in the x-direction, perpendicular to the long axis of the prisms. The coupling ratios calculated from the forward modeling at 912 Hz were converted to half-space apparent conductivities in the standard manner. The results across the central 1 km of the model are shown in Figure 7. The apparent conductivity shown in Figure 7a displays an anomaly of 26 mS/m above background across the first prism (A) at a depth of 50 m. The anomaly reduces to 7 mS/m across the second prism (B) at a depth of 150 m.

In Figure 7b the location of each prism is defined over a lateral scale length of about 45 m (prism A) and 60 m (prism B). These lengths are each less than the actual prism width of 100 m. For high resolution studies conducted with a flight line spacing of 200 m or less then the gridding interval may be of the same order as the lateral scale lengths defined above. Given these conditions it may be considered advantageous to include TDR levels with a mapping of conductive zones using two TDR intervals from 0° to 45° and from 45° to 90° as a general aid in the detection and definition of conductivity structure. For these types of bodies, the 90º contour line would represent the centre of the body and the 45º to 90º contour interval would provide a reasonable estimate of the extent of the body. It is acknowledged that, in detail, the lateral extent

of the positive TDR response will be governed by the depth of the body (e.g. Figure 7b).

5.3 Faulted half-space

The above two studies relate to laterally-compact, concealed, conductive zones. The behaviour of the TDR response in the case of a simple faulted half-space (i.e. two quarter spaces) is now considered. The EM response of a 1D distribution of conductivity that contains a vertical offset (e.g. a normal or reversed fault) will give rise to an anomaly across the fault. The characteristics of the anomaly will depend on the particular vertical conductivity distribution involved, and the depth and extent of the offset, together with the EM frequency, or range of frequencies, considered. In order to provide a generic example, it is useful to consider the limiting case of two vertically-uniform quarter spaces. The model comprises two large bodies that form effective EM quarter-spaces (defined from the surface to large depths). The modelling employed a differential equation approach developed by Sasaki (2001) for the forward modelling component of a 3D inversion scheme.

The conductivity of the two quarter spaces was set at 10 and 5 mS/m giving a conductivity contrast ratio of 2. Forward modeling of the airborne response was undertaken assuming a survey altitude of 50 m. Survey profiles (flight lines) were defined in the x-direction, perpendicular to the strike of the conductivity contrast. The coupling ratios calculated from the forward modeling at a frequency of 3005 Hz were then converted to half-space apparent conductivities in the standard manner. The results across the central 600m of the model are shown in Figure 8. The apparent conductivity (Figure 8a) tends to the true values of conductivity at large distances (300 m) from the fault located at the origin. Across the central interval between +/- 100 m, there is an ‘adjustment distance’ (Beamish 2004a) which defines the main gradient in conductivity due to the fault.

The TDR response, shown in Figure 8b, displays a zero at the fault location and tends to values of 90º above the more conductive structure and towards -90º above the more resistive structure. The behavior is analogous to the TDR characteristics observed across an equivalent magnetic quarter-space model (Salem *et al.* 2007) in which positive values of the TDR response are observed above the magnetic body. The behavior of the TDR response at distances greater than +/ 100 m is probably due to slight numerical inaccuracies in the EM modeling and transformation to conductivity values which are subsequently amplified when the TDR response is calculated.

In terms of the previously prescribed TDR contour interval (45º to 90º) for mapping both the outline and edge locations of compact conductive zones, it can be seen in Figure 7b that this interval would exclude correct edge detection in the case of simple faulted 1D conductivity distributions. As is indicated in Figure 7b by the infill zones, the option of contouring two intervals from 0º to 45º and from 45º to 90º would enable the two forms of edge responses to be mapped. With reference to Figure 8b, it can also be noted that a mapping of resistive features can also be achieved using the two equivalent negative zones of the TDR response.

6. Application of the TDR to survey data.

Although the main purpose of the present study relates to a consideration of spatial derivatives applied to conductivity data, the TDR response of the magnetic data is also considered.

6.1 The study area

As is evident from previous presentations of the data sets across the 20 x 20 km study area, non-geological, high-wavenumber noise sources are pervasive in both the magnetic and conductivity data sets. When the TDR response is obtained for such data, the noise gradients are given equal weight to geological gradients. For clarity of presentation we have upward-continued the data sets (shown in Figure 2) by 100 m (2 grid cells) before calculating the TDR response.

The TDR response of the reduced-to-pole, upward-continued magnetic data set is shown in Figure 9 using four 45 º contour intervals. Under the assumption of isolated, vertically-magnetised source bodies, the TDR zero values provide an estimate of the edge locations of such bodies. For positively-magnetised sources, the contour interval from 45º to 90º outlines the body. For reversely-magnetised bodies (e.g. the majority of dykes) the interval from -45º to -90º shows the extent of the body. The presence of a series of such dykes, towards the southern margin of the area, introduces a 'ridge-and-furrow' effect in the TDR response such that the amplitude characteristics (e.g. Figure 2) of the data need to be consulted. As discussed previously, the dykes and magnetic structure associated with the Lack Inlier provide high amplitude features that intersect in an oblique fashion, with considerable detailed complexity. In such circumstances both the processing and interpretation of the magnetic data remains challenging. The data would probably benefit from the application of further, more advanced, processing procedures, involving azimuthal and spectral filtering such as those undertaken in relation to the corresponding dyke swarm on Anglesey, North Wales, by Beamish and White (2011).

The TDR response of the upward-continued conductivity data (3125 Hz) set is shown in Figure 10 using four 45 º contour intervals. In keeping with the previous discussion, only the intervals from 0º to 45º and 45º to 90º are shown with infill. The geological/fault map from Figure 2a is shown as a reference background. Conductive zones are associated with the contour interval from 45º to 90º and, for these, data, the estimated edge location is assumed to be the 45º contour. The TDR response provides a uniform gain response across all the conductivity gradients as can be seen by comparing the shaded-relief images of Figure 4a,b with Figure 10. The advantage of the TDR response is that it is independent of horizontal gradient azimuth and, by virtue of the AGC, it summarises all the detectable conductive zones within and across the geological formations. Thus the relatively resistive Lack Inlier, bounded by highly conductive zones associated with its northern and southern margins, contains only a few, but potentially significant, much smaller amplitude conductive zones. The Carboniferous unit (grey in Figure 10) is seen to contain a

sinuous and extensive conductive feature at varying distances from the northern margin of the outcrop. The same conductive zone can be noted, to some degree, in the previous presentations of the conductivity data (Figures 2c and 4a,b). The width of the zone occupied by the TDR interval above 45º is generally 500 m or greater and would therefore be associated with the more extensive conductivity contrast of the type shown in Figure 8.

As with the magnetic data, the TDR conductivity response also equalises the response of geological and cultural gradients. High-wavenumber cultural perturbations from point sources are attenuated (but not necessarily removed) by upward-continuation however the quasi-linear responses of certain sections of roads (or road-edges possibly associated with service routes) remain as potential interpretation pitfalls. Such small amplitude/gradient responses exist in the basic data set (Figure 2a,b) however they are identified most clearly in the TDR response. This enables the TDR response to be used as an aid in the identification, and subsequent removal, of such features. The TDR response shown in Figure 10 is reproduced in Figure 11 with an additional map obtained from a database of road centre locations. The database contains attributes of road class (e.g. A, B, C and unclassified) and the road routes shown in Figure 11 contain all these classes.

Although the upward-continued TDR response shown in Figure 11 may not be optimised for the highest wavenumber detection, a series of zones, identified using ellipses, are indicated. The elliptic zones contain locations where there is a clear sustained association between the location of a road route and a positive (conductive) TDR response. It can be noted that these are largely minor B-roads and that the positive TDR response is only observed along a particular section of a road. The TDR response which generates a uniform gain for all such cultural (assumed) anomalies and takes into account all possible azimuths of such features, provides a robust method for their detection and, potentially, their removal.

In addition to the TDR responses associated with roads, a large number of compact, isolated responses are observed. At the scale shown, they have the appearance of scattered noise sources, such as those encountered in the magnetic data. In the magnetic case, the features are invariably associated with built-structures (buildings) containing magnetic content (Lahti *et al.* 2007). One such example is labelled C in Figure 11. The same large farm complex produces this cultural response previously noted in both data sets displayed in Figure 2. Elsewhere the compact conductivity TDR anomalies are largely associated with entirely rural areas (no buildings) and many exceed over 500 m in size. The significance of such features remains a topic that requires more detailed examination. The TDR detection attributes of such local scale responses is further illustrated later in this section.

6.2 The Tellus data set

In order to consolidate the concepts and results of applying the TDR response to AEM conductivity data, it is informative to consider the TDR responses obtained for the complete Tellus survey of Northern Ireland. At this scale, the TDR responses are too rich in detail to be effectively reproduced. Both magnetic and conductivity data sets

are therefore upward-continued by 200 m (4 grid cells) to attenuate the higher order wavenumber content. The main purpose here is to summarise and compare the application of the spatial derivatives embodied in the TDR when applied to potential field and non-potential field data. The Tellus magnetic and conductivity data sets have been described by Beamish and Young (2009) and Chacksfield (2010).

The TDR response of the upward-continued magnetic data is shown in Figure 12, with contour infill applied just to the -45º to 0º contour interval (blue) and the 0º to 45º contour interval (red). The contour interval from 45º to 90º is displayed in white simply for clarity. Presented in this way, the image reveals the edges of magnetic source bodies, irrespective of the direction of magnetisation. The NE area contains the Antrim Flood Basalts (Figure 1) which provide a highly complex magnetic response pattern. The upward-continued TDR response across the area reveals some deeper-seated features that potentially indicate some of the major vents associated with lava emplacement. Elsewhere the extensive dyke swarms are a pervasive feature of the magnetic response and can be separated into a number of groups based on character and age (Chacksfield 2010). In the west, a good example of superimposed shallow (dyke) and deep (basement) TDR estimated edge features is provided. Crossing the centre of the 20 x 20 km test study area (shown as a rectangle in Figure 12), is a regionally extensive basement feature with a NE-SW trend. Towards the NE, the edge abuts the Antrim Basalts showing a clear alignment with a fault (Tow Valley Fault, TVF). The edge feature, which can be traced over a distance of ~100 km and is associated with a large scale positively magnetised basement feature that extends south east as far as the Tempo-Sixmilecross Fault (TSF). The zero contour line corresponds to a previously discussed (though less well resolved) magnetic lineament referred to as the Fair Head- Clew Bay Line (Hutton 1987). The lineament is regarded as the south-westerly extension of the Highland Boundary fault in Scotland.

The TDR response of the upward-continued conductivity (3125 Hz) data is shown in Figure 13, with contour infill applied to the 0º to 45º contour interval (blue) and the 45º to 90º contour interval (red). In comparison with the magnetic information on spatial derivatives of Figure 12, the conductivity data, based on a focussed active geophysical measurement can be seen to provide only localised information. The TDR information essentially defines a series of conductive zones outlined by the 45º to 90º contour interval. The most extensive conductive zone is afforded by the sea-water body of Strangford Loch (SL, Figure 13). A detailed (3 x 3 km) area shown as a rectangle is studied later. The infilled (grey) polygons are locations of population with greater than 1000 inhabitants and are used to denote regulatory areas of high-fly and reduced confidence in the data.

One of the major features of the TDR conductivity response at this scale is the quasi-linear response from major cross-country energy transmission routes. They can be traced in the TDR response as they produce clean edge responses with associated negative (white) borders. Two examples (labelled P) are indicated in Figure 13. At this scale, they may be confused with geological responses such as those observed across the 20 x 20 km test area (large rectangle, Figure 13). Precise interpretation of all the geophysical data requires access to knowledge of all the potential sources of cultural interference. As with the magnetic data, the TDR conductivity response would ultimately be better constructed from a systematically decultured data set. Such

deculturing can take place using the observed coupling ratios and/or the derived conductivity data and remains to be undertaken in a comprehensive manner.

The extensive conductive zone across the test area (large rectangle) within the Carboniferous unit (Figure 2a) can now be traced more clearly by virtue of the additional upward-continuation. The feature either occupying a location along, or to the south of the northern edge of the Carboniferous outcrop, can now be traced for over 35 km. The feature can be seen to be just one of a series of conductive zones that extend across much of the south eastern area occupied by Carboniferous Limestones (Figure 1).

In order to bring together edge detection features observed in both magnetic and conductivity TDR responses, two extensive faults (the Tempo-Sixmilecross Fault, TSF and the Tow Valley Fault, TVF) are shown in Figures 12 and 13. Judging by the width of the magnetic TDR response *across* the TSF (Figure 12) the feature reflects the termination of a large-scale magnetic zone to the NW. The conductivity TDR response (Figure 13) indicates the existence of a narrow conductive zone *along* the TSF for the majority of its mapped length. At the termination of the TSF in the NE, the conductivity TDR would support an extension of the mapped fault by a further 14 km.

The Tow Valley Fault (TVF) in the NE is better termed a fault zone and juxtaposes the Upper Basalt Formation of the Antrim Flood Basalt to the NW with the Lower Basalt Formation to the SE (Mitchell 2004). The TDR magnetic response across the fault is very narrow (Figure 12) but as the fault has a considerable downthrow to the NW (Gibson 2004), a simple interpretation of the TDR magnetic response may not be justified. The conductivity response (Figure 13) indicates a quasi-continuous conductive zone along its entire length. At the termination of the mapped fault in the SW, the TDR conductivity response suggests in would be possible to continue/extend the fault and connect it with a splay of the TSF (marked S in Figure 13). It is evident that the two data sets contain distinct and complementary information.

6.3 A detailed example

The study of the conductivity data from the test area revealed a large number of isolated conductive zones that could be identified in the TDR response. Many of the responses are not associated with obvious signs of cultural influences. The inherent automatic gain control of the TDR function implies that small scale conductivity contrasts have the potential to be identified. The theoretical modelling of the TDR response revealed that conductivity contrasts as low as a factor of two may be identified in the TDR response. To further assess the characteristics of the TDR response at the local scale, an area that provides a degree of control in relation to known conductivity boundaries is now considered. The detailed example is taken from a 3 x 3 km area on the western margin of Strangford Lough (SL and rectangle, Figure 13). The area contains a number of islands typical of drowned drumlin topography. The water is assumed to be fully saline but detailed inshore bathymetry is not available. The maximum water depth is expected to be less than 10 m with each island offering differing shelving characteristics.

The topographic map, together with the 200 m flight line sampling, is shown in Figure 14. The main coastal zone tracks the western side of the area and contains a number of inlets. The largest island (Conley) lies just offshore and a further 11 islands are identified further offshore. The TDR conductivity response, at a frequency of 3125 Hz, is contoured, as previously, using two intervals from 0º to 45º (blue) and from 45º to 90º (red). In this case, no upward-continuation has been applied and the contour map has been obtained using a grid cell size of 50 x 50 m. The TDR response is overlaid on the topographic map in Figure 13 with the red (45º to 90º) interval made transparent to allow the full topographic map to be viewed. The fully transparent areas of the TDR response contain the interval from 0º to -90º and, presented in this manner, outline resistive zones in a conductive environment. As a technical note it would be equally possible, having obtained the conductivity TDR response, to 'map' resistive zones using the contour interval from 0º to -90º.

All the offshore islands with the exception of Parton Island which lies centrally between two adjacent flight lines produce clear resistive zones in the TDR response. At this scale, the actual data sampling and associated electromagnetic footprints of the flight lines in relation to the shape of the body plays a significant role in the correct detection of the edges of conductivity contrasts. As is often the case, a number of the smaller features appear beneath a single flight line and, in this case, body dimensions are generally best resolved along the axis of the flight line. Although the example chosen inevitably involves very large conductivity contrasts, the principle of the detection at much lower conductivity contrasts is a component part of the use of the TDR response. It could therefore be anticipated that small scale, low contrast environmental features in the landscape may be investigated using the TDR approach.

7. Discussion

This study has considered a number of ways in which the application of spatial derivatives can be used to enhance the mapping of conductivity data sets to better define conductive/resistive zones and their edges. All the techniques considered are established practice in enhancing the information content of potential field data.

Non-potential field data are generated by active fields and, in contrast to potential field measurements, provide a localised and compact scale of subsurface assessment. This leads to a distinction in the case of wavenumber content when extensive data sets are considered. This has been demonstrated by comparing and contrasting the application of spatial derivatives to jointly obtained magnetic and conductivity data obtained by airborne surveying. The performance of shaded-relief algorithms, the analytic signal amplitude (ASA), upward continuation and the tilt derivative have been considered. One advantage of ASA processing is that the information is independent of azimuth and it provides a numerical assessment of the total gradients in the data. A disadvantage is that the more subtle spatial continuity of gradient information provided by the shaded relief image is lost. The ASA has a potential role to play in the identification and removal of cultural perturbations.

A number of the procedures, particularly that of vertical continuation have been considered useful only to potential fields since they have an established basis in terms of existing theory. It has been noted that, provided the same transform is used only in the context of a filtering operation, then it can be usefully applied to other non-potential field data sets. A small degree of upward continuation has proved effective at attenuating localised, high-wavenumber content (often associated with noise) when applied to conductivity data. The same form of low-order (a few grid intervals) filtering is often used, for similar purposes, in magnetic data processing as a prelude to the calculation of higher-order derivatives.

The tilt derivative as applied to electromagnetic conductivity data has been studied in a series of theoretical studies. The studies demonstrate that the TDR can be used in the mapping of at-surface and concealed structural edges of conductive/resistive zones. A mapping of the TDR contour intervals from 0º to 45º and 45º to 90º is recommended. Having obtained a TDR response from conductivity information, it is also possible to provide a TDR of resistive zones using the equivalent negative response intervals. The width of the TDR response across a conductivity boundary increases with the depth of the boundary. Although in some highly simplified circumstances, this behaviour might be used to infer some depth related *mapping* information, in the general case depth dependent behaviour is better examined using information across multiple frequencies.

The TDR modeling studies have indicated the simplicity of the technique in relation to the detection of concealed conductive zones having a range of response amplitudes. In the airborne case, the lowest frequency (or latest time) offers the greatest potential for summarising the outlines of conductive domains across the largest range of depths. It can equally be applied to each of the half-space conductivity data sets individually.

Three case studies have considered the application of the TDR to conductivity data across a range of scales. A more complete geological interpretation of these data is beyond the scope of this paper and only a few limited but significant features have been noted. The inherent AGC of the technique normalizes the detection and definition of both strong and weak subsurface conductivity contrasts. This feature has been found to be particularly useful when applied to larger scale data sets, such as the complete Tellus survey, in relation to mapping the spatial attitude and continuity of regional scale features. A specific geological application of the TDR to the detection of conductive zones, at various depths, across the Lower Palaeozoic terrane of Northern Ireland (the greywacke unit in Figure 1) is described more fully by Beamish *et al.* (2010).

The use of spatial derivatives inevitably results in a degree of noise (cultural perturbation) amplification. As is demonstrated in the case studies, this applies equally to magnetic and conductivity data sets although the nature of the perturbations may differ. The noise sources influence all of the derivative mapping of the geophysical information from shaded-relief procedures through to the tilt derivative. All such procedures would ultimately be better generated from systematically decultured data sets. While such procedures already exist in the magnetic case, the present study goes some way to indicate the level of complexity that would arise when establishing an equivalent comprehensive deculturing of electromagnetic data.

In the case of magnetic data processing, a comprehensive set of spatial derivative procedures exist that assist with interpretation of the basic data set. Typically a range of these procedures, rather than a single procedure, is applied since each survey may comprise very different structural and signal-to-noise characteristics. The study has demonstrated the extension of these procedures to non-potential field data, and again, it is anticipated that a range of spatial derivative processing options should be considered.

8. Acknowledgements

My thanks go to the two referees and Editors for their efforts in improving the original submission. The data used in the study come from the Tellus Project which was funded by DETI and by the Building Sustainable Prosperity scheme of the Rural Development Programme (Department of Agriculture and Rural Development of Northern Ireland). Topographic map data based upon Ordnance Survey of Northern Ireland's® data with the permission of the Controller of Her Majesty's Stationery Office, © Crown copyright and database rights MOU205.This report is published with the permission of the Executive Director, British Geological Survey (NERC).

9. References

Beamish D. 2002. The canopy effect in airborne EM. Geophysics 67, 1720-1728.

Beamish D. 2004a. 3D modeling of near-surface, environmental effects on AEM data. Journal of Applied Geophysics 32, 213–217.

Beamish D. 2004b. Airborne EM skin depths. Geophysical Prospecting 52, 439-449.

Beamish D., Kimbell G.S., Stone P. and Anderson T.B. 2010. Regional conductivity data used to reassess Lower Palaeozoic structure in the Northern Ireland sector of the Southern Uplands–Down-Longford terrane. Journal of the Geological Society, London 167. 1–9.

Beamish D. and White J.C. 2011. Aeromagnetic data in the UK: a study of the information content of baseline and modern surveys across Anglesey, North Wales. Geophysical Journal International 184, 171-190.

Beamish D. and Young M. 2009. Geophysics of Northern Ireland: the Tellus effect. First Break 27, 43-49.

Blakely R.J. 1995. Potential Theory in Gravity and Magnetic Applications. Cambridge University Press. ISBN 052 41508X.

Blakely R. J. and Simpson R.W. 1986, Approximating edges of source bodies from magnetic or gravity anomalies. Geophysics 51, 1494-1498.

Chacksfield B.C. 2010. A preliminary interpretation of Tellus airborne magnetic and electromagnetic data for Northern Ireland. British Geological Survey Internal Report, IR/07/041.

Cooper G. R. J. Combrinck, M. and Cowan D.R. 2004. The application of Euler deconvolution to airborne EM data: 17th ASEG Geophysical Conference and Exhibition, Sydney, Extended Abstracts.

Cooper G. R. J. and Cowan D.R. 2006. Enhancing potential field data using filters based on the local phase. Computers and Geosciences 32, 1585–1591.

Cooper G. R. J. and Cowan D.R. 2008. Edge enhancement of potential-field data using normalized statistics. Geophysics 73, H1-H4.

Fairhead J.D. Green C.M. Verduzco B. and Mackenzie C. 2004. A new set of magnetic field derivatives for mapping mineral prospects: 17th ASEG Geophysical Conference and Exhibition, Sydney, Extended Abstracts.

Florio G. Fedi M. and Pasteka R. 2006. On the application of Euler deconvolution to the analytic signal. Geophysics 71, L87-L93.

Fraser D.C. 1978. Resistivity mapping with an airborne multicoil electromagnetic system. Geophysics 43, 144–172.

Gibson P.J. 2004. Geophysical characteristics of the Tow Valley fault in north-east Ireland. Irish Journal of Earth Sciences 22, 1-13.

Habashy T. M. Groom R.W. and Spies B. R. 1993. Beyond the Born and Rytov Approximations: A Nonlinear Approach to Electromagnetic Scattering. Journal of Geophysical Research 98, 1759-1775.

Horn B.K.P. 1982. Hill shading and the reflectance map. Geoprocessing 2, 65–146.

Hutton D. W. H. 1987. Strike-slip terranes and a model for the evolution of the British and Irish Caledonides. Geological Magazine 124, 405-425.

Kovacs A. Holladay J.S. and Bergeron C.J. Jr. 1995. The footprint/ altitude ratio for helicopter electromagnetic sounding of seaice thickness: Comparison of theoretical and field estimates. Geophysics 60**,** 374–380.

Lahti M. Beamish D. Cuss R.J. and Williams J. 2007. Deculturing of the Northern Ireland Tellus magnetic data. British Geological Survey Technical Report IR/07/147.

Lahti I. and Karinen T. 2010. Tilt derivative multiscale edges of magnetic data. The Leading Edge 29, 24–29.

Leväniemi H. Beamish D. Hautaniemi H. Kurimo M. Suppala, I. Vironmäki J. Cuss R.J. Lahti M. and Tartaras E. 2009. The JAC airborne EM system AEM-05: Journal of Applied Geophysics 67, 219-233.

Li X. 2003. On the use of different methods for estimatimg magnetic depth. The Leading Edge 22, 1090-1099.

Liu G. and Becker A. 1990. Two-dimensional mapping of sea-ice keels with airborne electromagnetics. Geophysics 55**,** 239–248.

McGillivray P.R. Oldenburg D.W. Ellis R.G. and Habashy T.M. 1994. Calculation of sensitivities for the frequency domain electromagnetic problem. Geophysical Journal International 116**,** 1–4.

Miller H. G. and Singh, V. 1994. Potential field tilt - A new concept for location of potential field sources. Journal of Applied Geophysics 32, 213–217.

Mitchell W.I. (ed.) 2004. The geology of Northern Ireland: Our Natural Foundation. Geological Survey of Northern Ireland, Belfast. ISBN 0852724543.

Nabighian M.N. 1972. The analytical signal of two-dimensional magnetic bodies with polygonal cross-section: its properties and use for automated anomaly interpretation. Geophysics 37, 507-517.

Nabighian M.N. Grauch, V. J. S. Hansen R. O., LaFehr T. R. Li, Y. Peirce J. W. Phillips J.D. and Ruder M. E. 2005. The historical development of the magnetic method in exploration. Geophysics 70, 33ND-61ND.

Parnell J. Earls G. Wilkinson J.J. Hutton D.H.W. Boyce A.J. Fallick A.E. Ellam R.M. Gleeson S.A. Moles N.R. Carey P.F. and Legg I. 2000. Regional fluid flow and gold mineralization in the Dalradian of the Sperrin Mountains, Northern Ireland. Economic Geology 95, 1380-1416.

Reid A.B. Allsop, J.M. Granser H. Millet A.J. and Somerton, I.W. 1990. Magnetic interpretation in three dimensions using Euler deconvolution. Geophysics 55, 80-91.

Roest W.R. Verhoef J. Pilkington M. 1992. Magnetic interpretation using 3-D analytic signal. Geophysics 57,116-125.

Roy A. 1966. Downward continuation and its application to electromagnetic data interpretation. Geophysics 31, 167-184.

Salem A. Williams S. Fairhead D. Ravat D. and Smith R. 2007. Tilt-depth method: a simple depth estimation method using first-order magnetic derivatives. The Leading Edge 26, 1502–1505.

Salem A. Williams S. Fairhead D. Smith R. and Ravat D. 2008. Interpretation of magnetic data using tilt-angle derivatives. Geophysics 73, L1-L10.

Sasaki Y. 2001. Full 3-D inversion of electromagnetic data on PC. Journal of Applied Geophysics 46, 45– 54.

Suppala I. Oksama M. and Hongisto H. 2005. GTK airborne EM system: characteristics and interpretation guidelines. In: Aerogeophysics in Finland 1972–2004: Methods, System Characteristics and Applications, (ed. M-L Airo) Geological Survey of Finland, Special Paper 39,103–118. ISBN 9516909159,

Thompson D. T. 1982. EULDPH: A new technique for making computer-assisted depth estimates from magnetic data. Geophysics 47, 31-37.

Tølbøll R.J. and Christensen N.B. 2006. Robust 1D inversion and analysis of helicopter electromagnetic (HEM) data. Geophysics 71, 53-62.

Weidelt P. 1981, Dipolinduktion in einer dünnen platte mit leitfähiger umgebung und deckschicht: Report 89727, BGR, Hannover.

Verduzco B. Fairhead J.D. Green C.M. and Mackenzie C. 2004. New insights into magnetic derivatives for structural mapping. The Leading Edge 23, 116–119.

Figure captions

Figure 1. Survey area, location map (top right). Main map shows simplified geological map of Northern Ireland (1:650k) with outer line defining the extent of the Tellus airborne geophysical survey. Two rectangles outline detailed data sets discussed in the text. W refers to large water bodies.

Figure 2. 20 x 20 km test area, with all images shown in perspective view looking north.
(a) 1:250k geological map with additional fault lines (dotted) and Omagh Thrust (OT) and Cool Fault (CF) noted. DALR=Dalradian, CARB=Carboniferous, DEV=Devonian, D=Dyke. Cross-hatch denotes population centres.
(b) Total Magnetic Intensity (TMI), reduced-to-pole, anomaly image. Linear colour scale, limited to +/- 200 nT.
(c) Apparent half-space conductivity (3125 Hz). Linear colour scale, limited from 0.5 to 50 mS/m.
Letter C in images (b) and (c) denotes a cultural perturbation discussed in the text.

Figure 3. Radially/azimuthally averaged power spectra of test area magnetic and conductivity data shown in Figure 2. Lines with symbols are power spectra following upward-continuation of data by 100 m (two grid cells).

Figure 4. Shaded relief images of test area (20 x 20 km) conductivity (a,b) and magnetic (c,d) data. Sun elevation is 45º throughout. Sun azimuth is 135º (shown by arrows) in (a) and (c). Sun azimuth is 45º (shown by arrows) in (b) and (d).

Figure 5. Plots of the analytic signal amplitude (ASA) of test area (20 x 20 km) data. Contour lines are coloured from low values (black) to high values using increasingly lighter grey. (a) Magnetic data. Amplitudes from 0.001 nT/m (black) to 8.9 nT/m (light grey), using a contour interval of 0.1 nT/m. (b) Conductivity data. Amplitudes

from 0.0001 mS/m^2 (black) to 11.3 mS/m^2 (light grey), using a contour interval of 0.1 mS/m^2.
Images (c) and (d) are ASA following upward-continuation of the data by 100 m (two grid cells). (c) Magnetic data. Amplitudes from 0.0003 nT/m (black) to 1.6 nT/m (light grey), using a contour interval of 0.1 nT/m. (d) Conductivity data. Amplitudes from 0.00009 mS/m^2 (black) to 1.2 mS/m^2 (light grey), using a contour interval of 0.1 mS/m^2.

Figure 6. Results obtained from thin-sheet modelling of a vertical conducting plate located below the origin. The airborne response of the system described in the text was calculated. The frequency used is 912 Hz. (a) Half-space apparent conductivity with the upper surface of the plate at 4 depths. (b) The tilt derivative (TDR) of the apparent conductivity data with the upper surface of the plate at 4 depths. Two 45° zones of the positive TDR response are shown shaded. (c) The total horizontal derivative of the tilt (THDR) with the upper surface of the plate at the two limiting depths of the study.

Figure 7. Results obtained from finite prism modelling of two conducting bodies at depths (upper surfaces) of 50 m (A) and 150 m (B). The airborne response of the system described in the text was calculated. The frequency used is 912 Hz. Each prism is 100 m wide, as denoted by the horizontal arrows. The centre of prism A is located at -250 m and prism B is located at +250 m from the origin. (a) Half-space apparent conductivity. (b) The tilt derivative (TDR) of the apparent conductivity data. Two 45° zones of the positive TDR response are shown shaded.

Figure 8. Results obtained from extended prism modelling of two bodies representing two quarter spaces. The bodies have conductivities of 10 mS/m and 5 mS/m as shown. The airborne response of the system described in the text was calculated. The frequency used is 3005 Hz. (a) Half-space apparent conductivity. (b) The tilt derivative (TDR) of the apparent conductivity data. Two 45° zones of the positive TDR response are shown shaded.

Figure 9. Plot of the tilt derivative (TDR) of the upward continued (100 m) magnetic data across the test area (20 x 20 km). TDR response contoured using an interval of 45º.

Figure 10. The tilt derivative (TDR) of the upward continued (100 m) conductivity data across the test area (20 x 20 km). TDR response contoured using an interval of 45º with only two intervals shown with infill. Shown on the background geological map from Figure 2a.

Figure 11. The tilt derivative (TDR) of the upward continued (100 m) conductivity data across the test area (20 x 20 km), same as shown in Figure 10. Background lines are from a database of the centre-lines of roads across the area. Letter C and arrow denotes a cultural perturbation discussed in the text. Ellipses with transparent infill indicate zones in which positive values of the TDR appear associated with roads.

Figure 12. Tilt derivative (TDR) of the upward continued (200 m) magnetic data for the Tellus survey. TDR response contoured using an interval of 45º with only two intervals shown with infill. Location of 20 x 20 km test area shown as a rectangle. Location of two faults (TVF=Tow Valley Fault, TSF= Tempo-Sixmilecross Fault) shown with green dotted lines.

Figure 13. Tilt derivative (TDR) of the upward continued (200 m) conductivity data for the Tellus survey. Frequency is 3125 Hz and data has been cut to the coastline. TDR response contoured using an interval of 45º with only two intervals shown with infill. Location of 20 x 20 km test area shown as a rectangle. A second 3 x3 km rectangle is shown adjacent to Strangford Lough (SL). Location of two faults (TVF=Tow Valley Fault, TSF= Tempo-Sixmilecross Fault) shown with green dotted lines. Areas with grey infill denote population centres. P denotes an example of a major power line response.

Figure 14. Tilt derivative (TDR) of the conductivity data across a 3 x 3 km test area (shown in Figure 13). Frequency is 3125 Hz and 200 m flight lines are shown as dots. TDR response contoured using an interval of 45º with only two intervals shown with

infill. The infilled contour interval from 45º to 90º is transparent. The background is a 1:50k topographic map showing the western coast of Strangford Lough and a series of offshore islands/rocks. Map contains grid squares at a 1 km interval for scale.

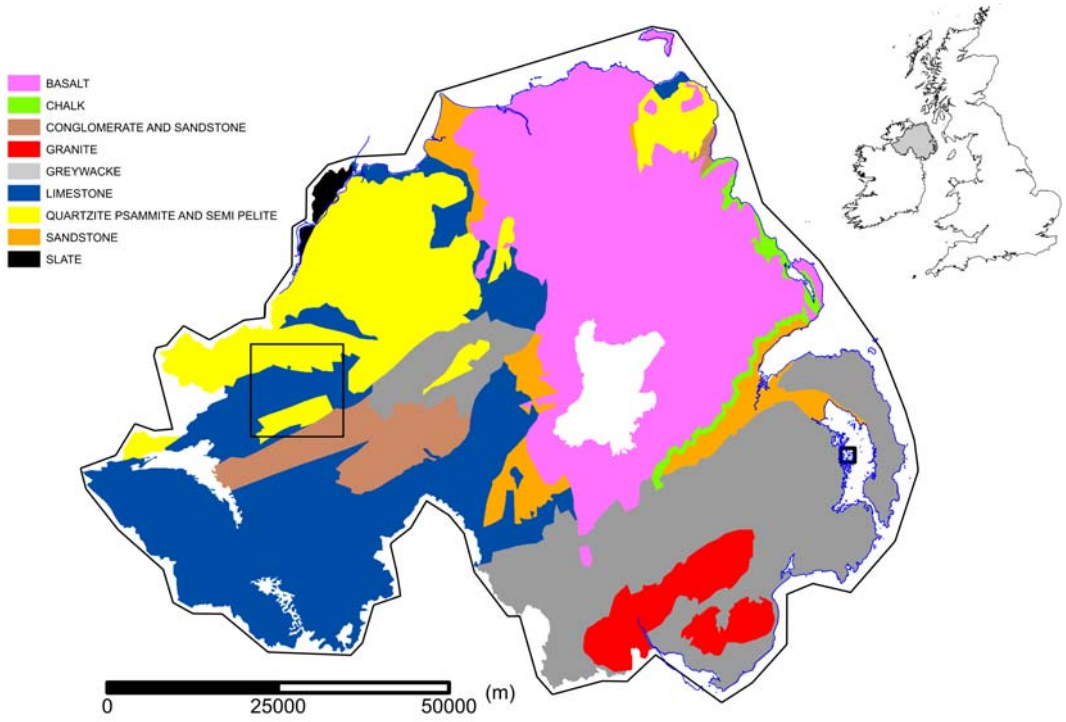

Figure 1. Survey area, location map (top right). Main map shows simplified geological map of Northern Ireland (1:650k) with outer line defining the extent of the Tellus airborne geophysical survey. Two rectangles outline detailed data sets discussed in the text. W refers to large water bodies.

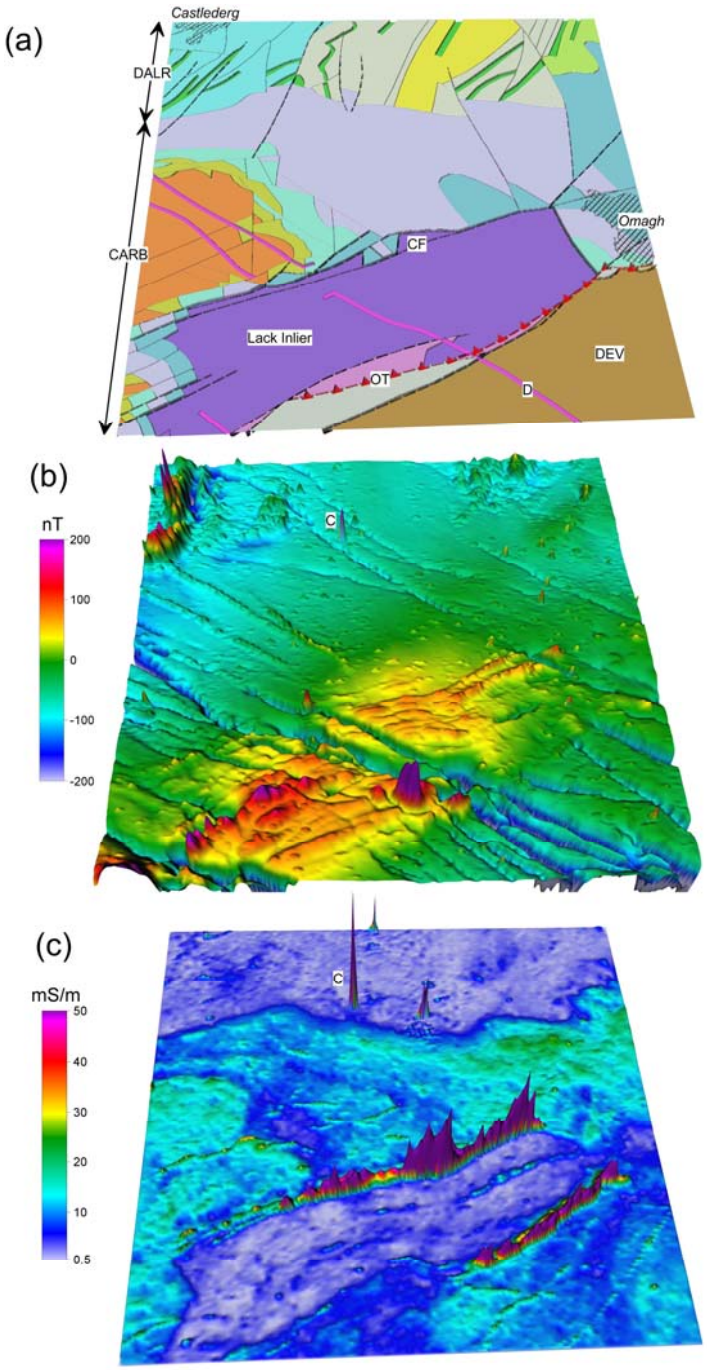

Figure 2. 20 x 20 km test area, with all images shown in perspective view looking north.
(a) 1:250k geological map with additional fault lines (dotted) and Omagh Thrust (OT) and Cool Fault (CF) noted. DALR=Dalradian, CARB=Carboniferous, DEV=Devonian, D=Dyke. Cross-hatch denotes population centres.
(b) Total Magnetic Intensity (TMI), reduced-to-pole, anomaly image. Linear colour scale, limited to +/- 200 nT.
(c) Apparent half-space conductivity (3125 Hz). Linear colour scale, limited from 0.5 to 50 mS/m.
Letter C in images (b) and (c) denotes a cultural perturbation discussed in the text.

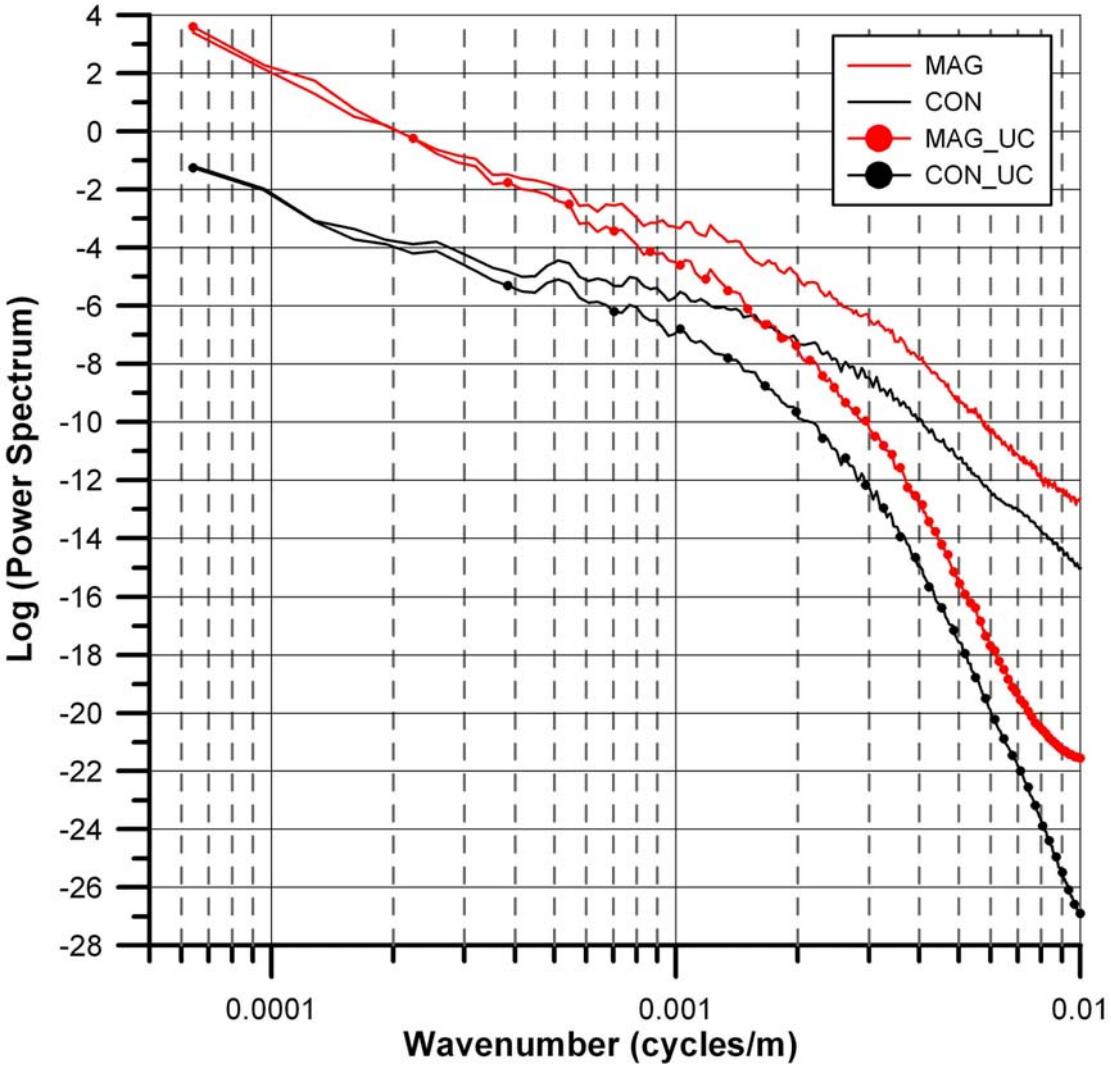

Figure 3. Radially/azimuthally averaged power spectra of test area magnetic and conductivity data shown in Figure 2. Lines with symbols are power spectra following upward-continuation of data by 100 m (two grid cells).

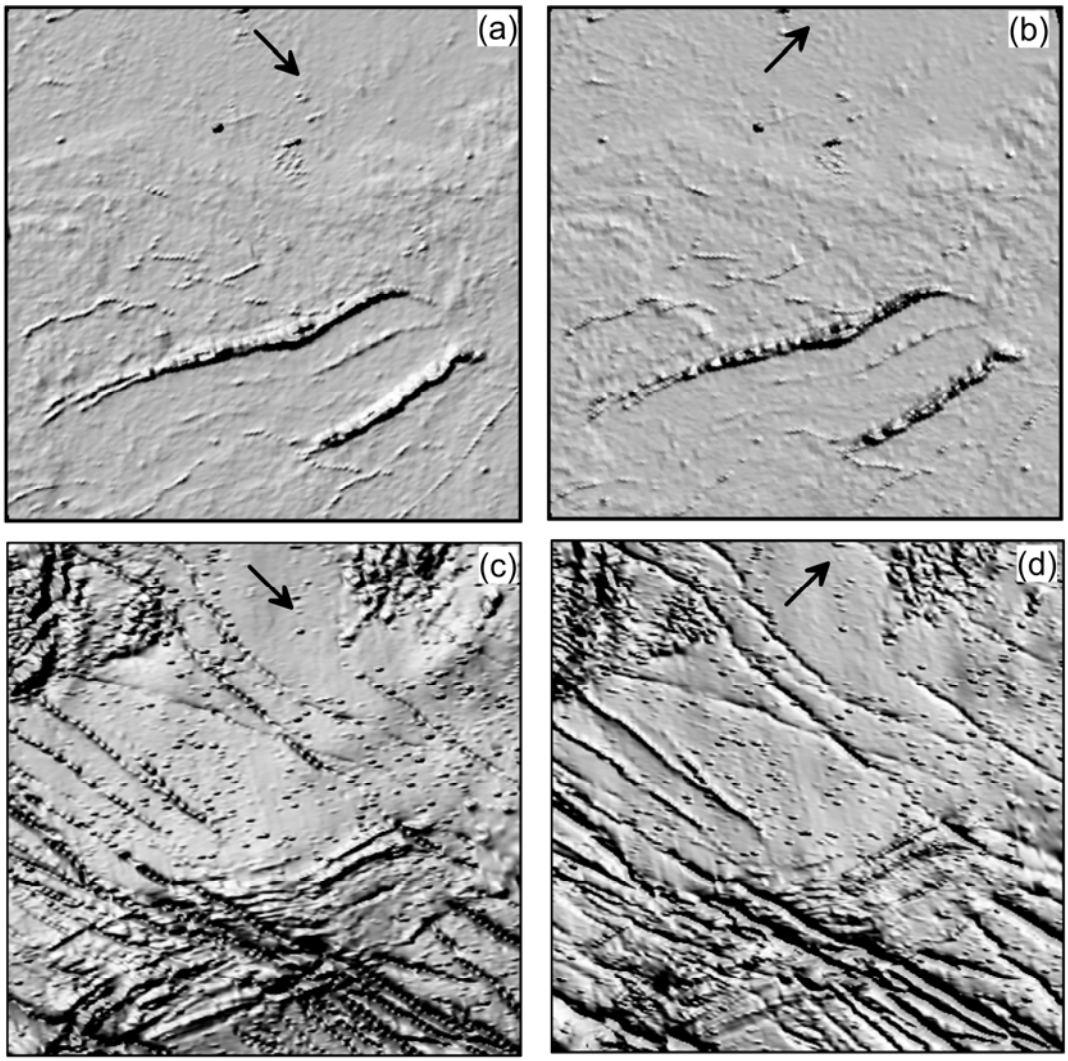

Figure 4. Shaded relief images of test area (20 x 20 km) conductivity (a,b) and magnetic (c,d) data. Sun elevation is 45º throughout. Sun azimuth is 135º (shown by arrows) in (a) and (c). Sun azimuth is 45º (shown by arrows) in (b) and (d).

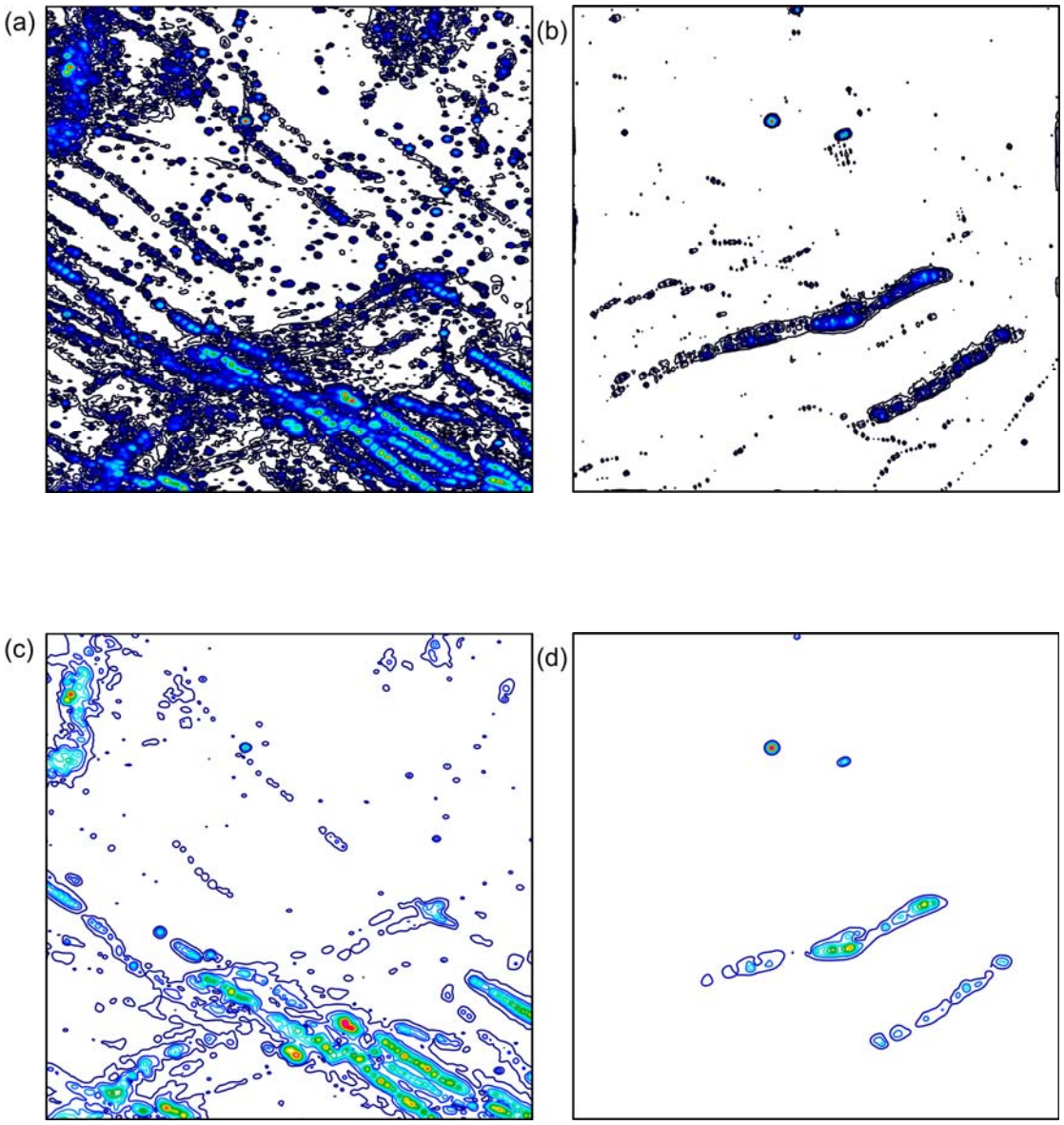

Figure 5. Plots of the analytic signal amplitude (ASA) of test area (20 x 20 km) data. Contour lines are coloured from low values (black) to high values using increasingly lighter grey. (a) Magnetic data. Amplitudes from 0.001 nT/m (black) to 8.9 nT/m (light grey), using a contour interval of 0.1 nT/m. (b) Conductivity data. Amplitudes from 0.0001 mS/m^2 (black) to 11.3 mS/m^2 (light grey), using a contour interval of 0.1 mS/m^2.
Images (c) and (d) are ASA following upward-continuation of the data by 100 m (two grid cells). (c) Magnetic data. Amplitudes from 0.0003 nT/m (black) to 1.6 nT/m (light grey), using a contour interval of 0.1 nT/m. (d) Conductivity data. Amplitudes from 0.00009 mS/m^2 (black) to 1.2 mS/m^2 (light grey), using a contour interval of 0.1 mS/m^2.

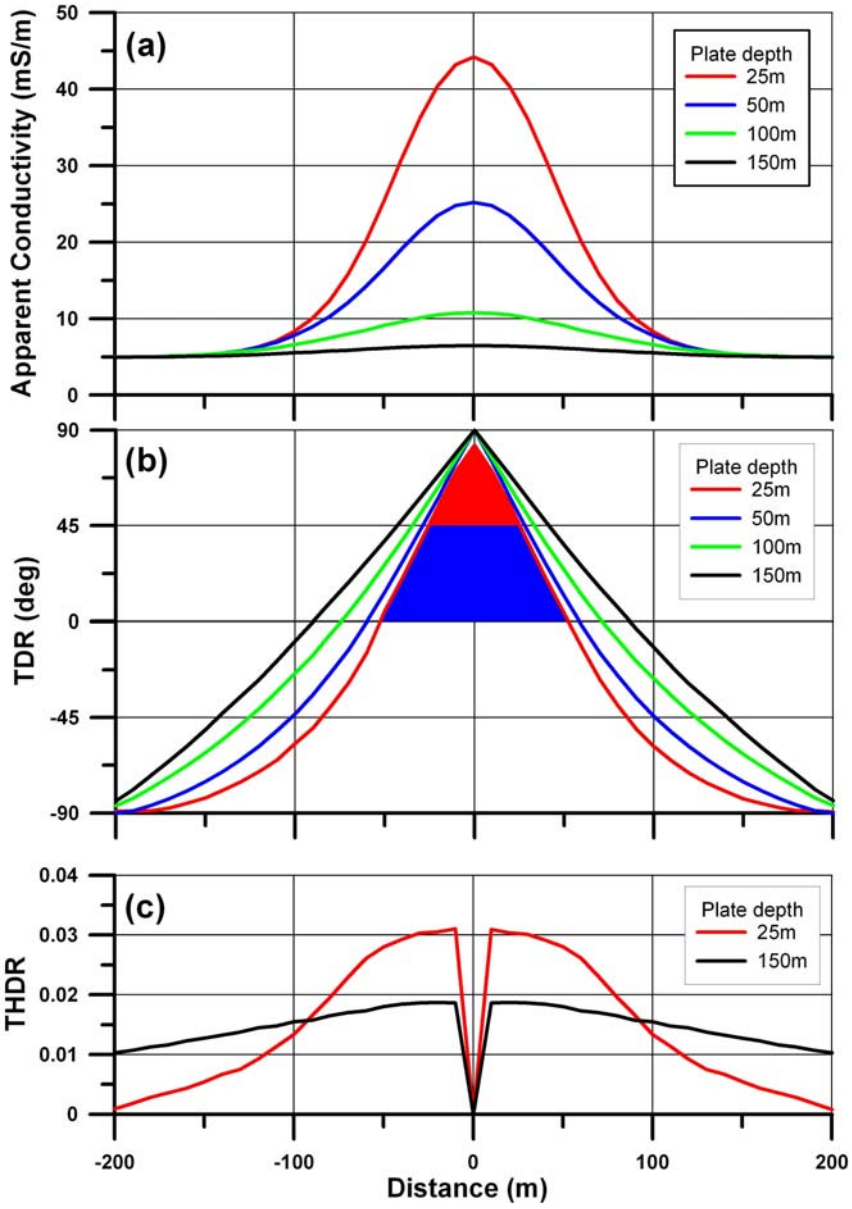

Figure 6. Results obtained from thin-sheet modelling of a vertical conducting plate located below the origin. The airborne response of the system described in the text was calculated. The frequency used is 912 Hz. (a) Half-space apparent conductivity with the upper surface of the plate at 4 depths. (b) The tilt derivative (TDR) of the apparent conductivity data with the upper surface of the plate at 4 depths. Two 45° zones of the positive TDR response are shown shaded. (c) The total horizontal derivative of the tilt (THDR) with the upper surface of the plate at the two limiting depths of the study

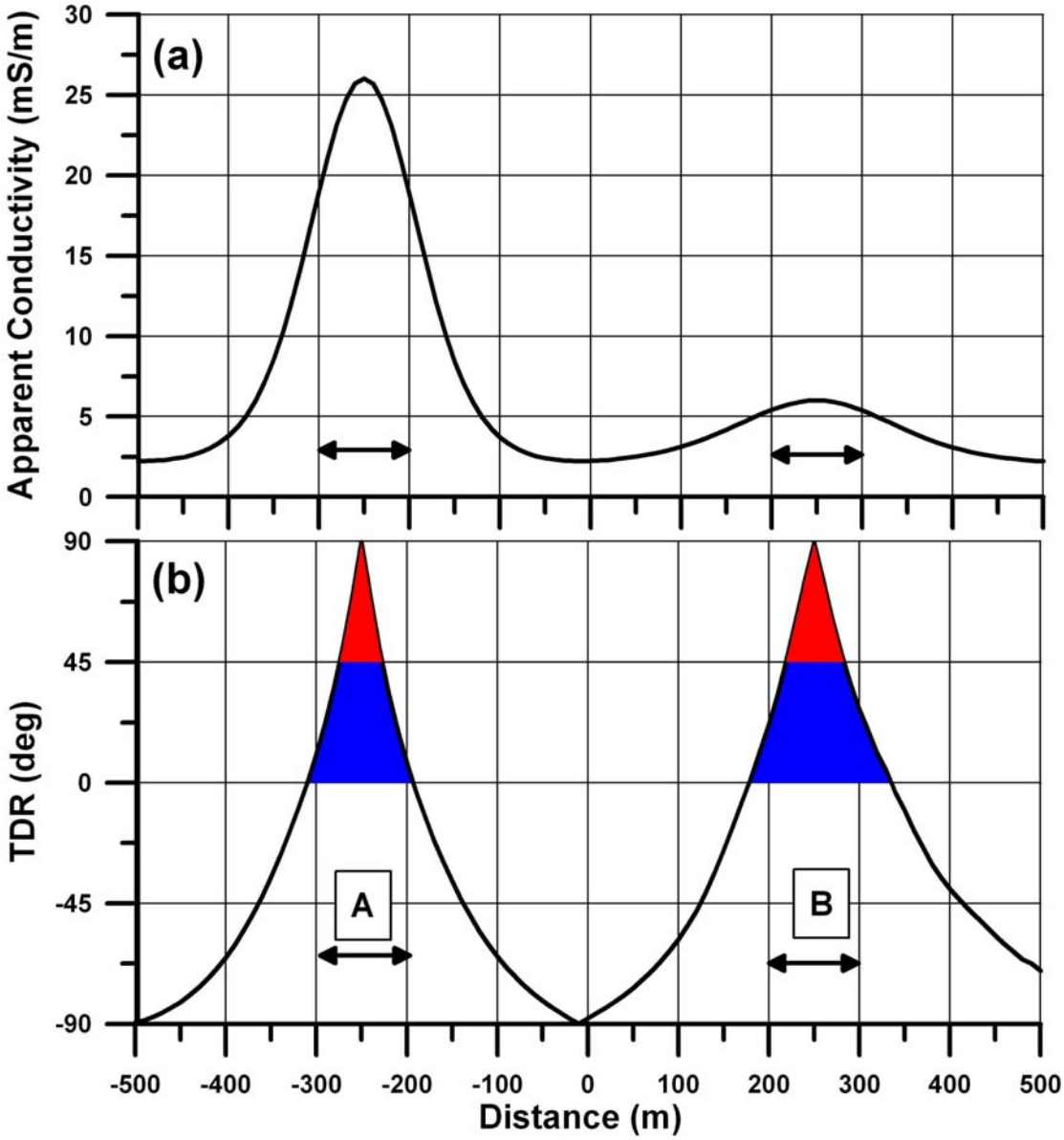

Figure 7. Results obtained from finite prism modelling of two conducting bodies at depths (upper surfaces) of 50 m (A) and 150 m (B). The airborne response of the system described in the text was calculated. The frequency used is 912 Hz. Each prism is 100 m wide, as denoted by the horizontal arrows. The centre of prism A is located at -250 m and prism B is located at +250 m from the origin. (a) Half-space apparent conductivity. (b) The tilt derivative (TDR) of the apparent conductivity data. Two 45° zones of the positive TDR response are shown shaded.

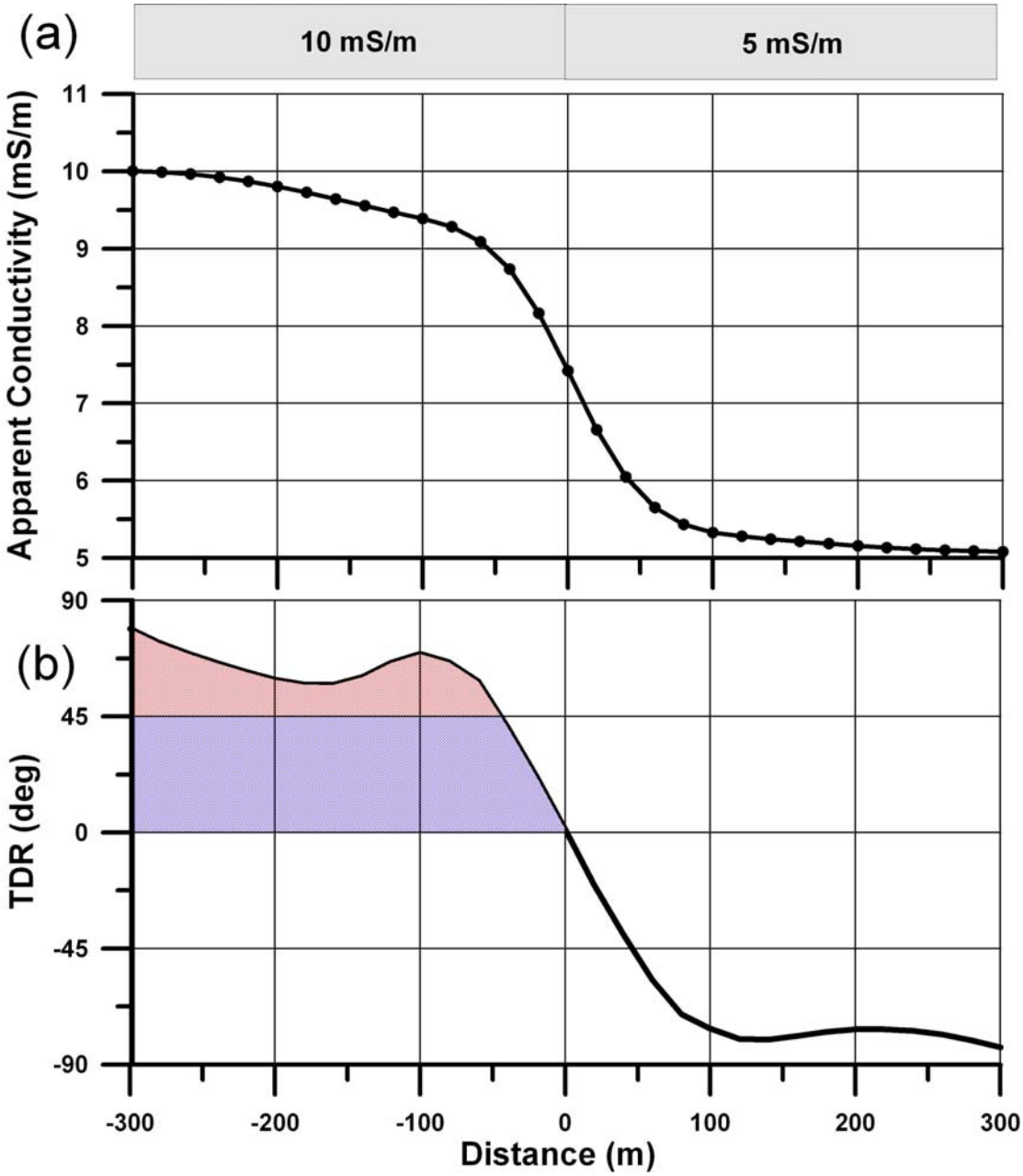

Figure 8. Results obtained from extended prism modelling of two bodies representing two quarter spaces. The bodies have conductivities of 10 mS/m and 5 mS/m as shown. The airborne response of the system described in the text was calculated. The frequency used is 3005 Hz. (a) Half-space apparent conductivity. (b) The tilt derivative (TDR) of the apparent conductivity data. Two 45° zones of the positive TDR response are shown shaded.

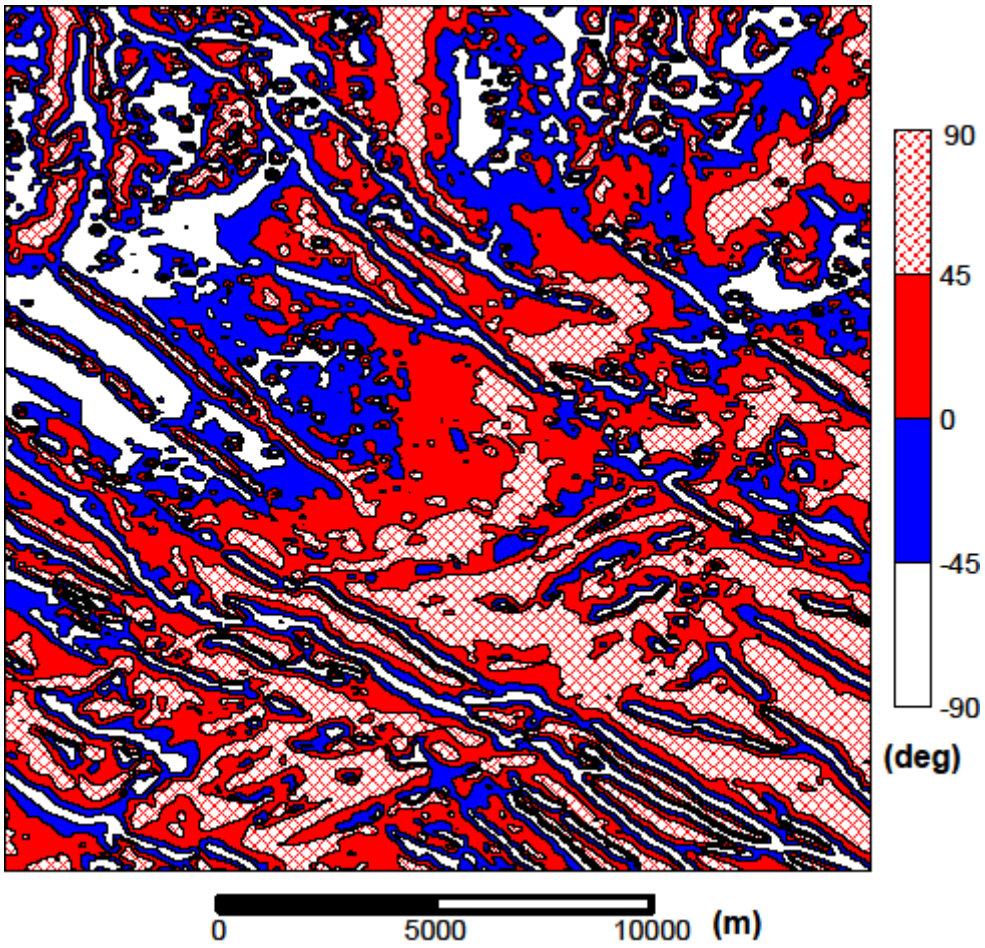

Figure 9. Plot of the tilt derivative (TDR) of the upward continued (100 m) magnetic data across the test area (20 x 20 km). TDR response contoured using an interval of 45º.

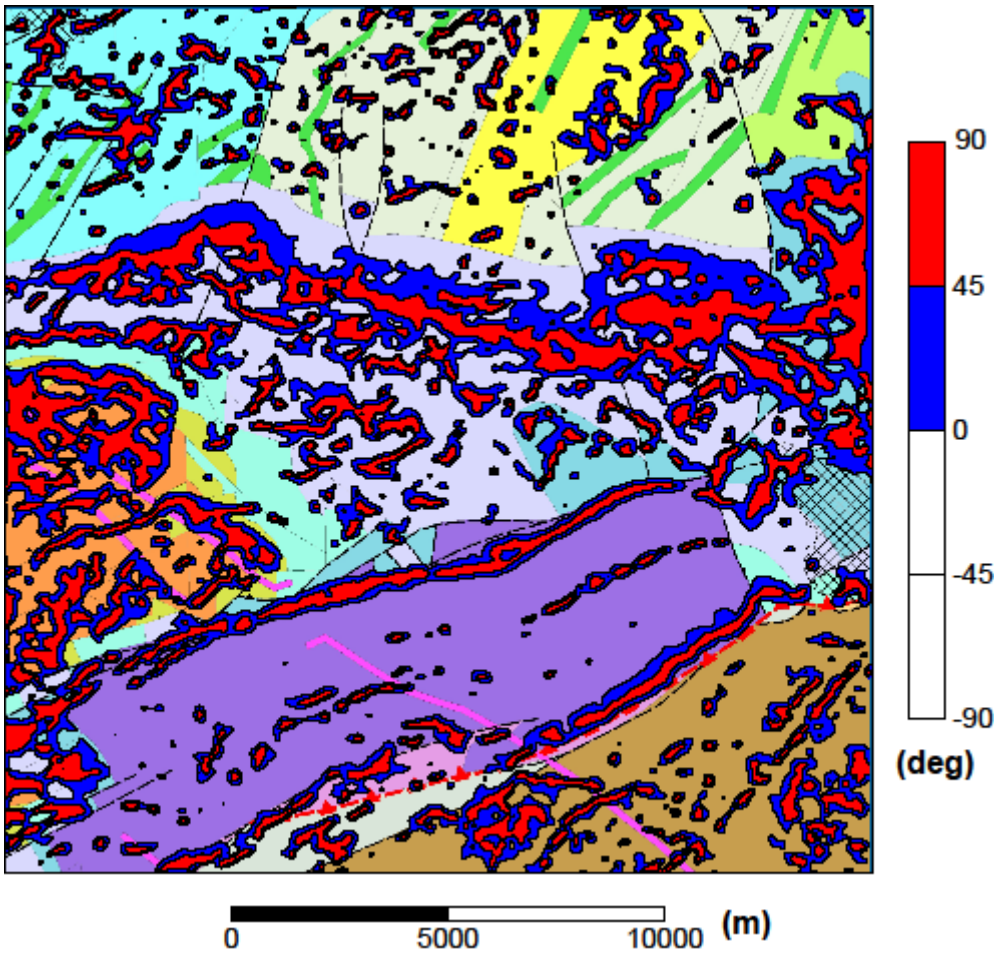

Figure 10. The tilt derivative (TDR) of the upward continued (100 m) conductivity data across the test area (20 x 20 km). TDR response contoured using an interval of 45º with only two intervals shown with infill. Shown on the background geological map from Figure 2a.

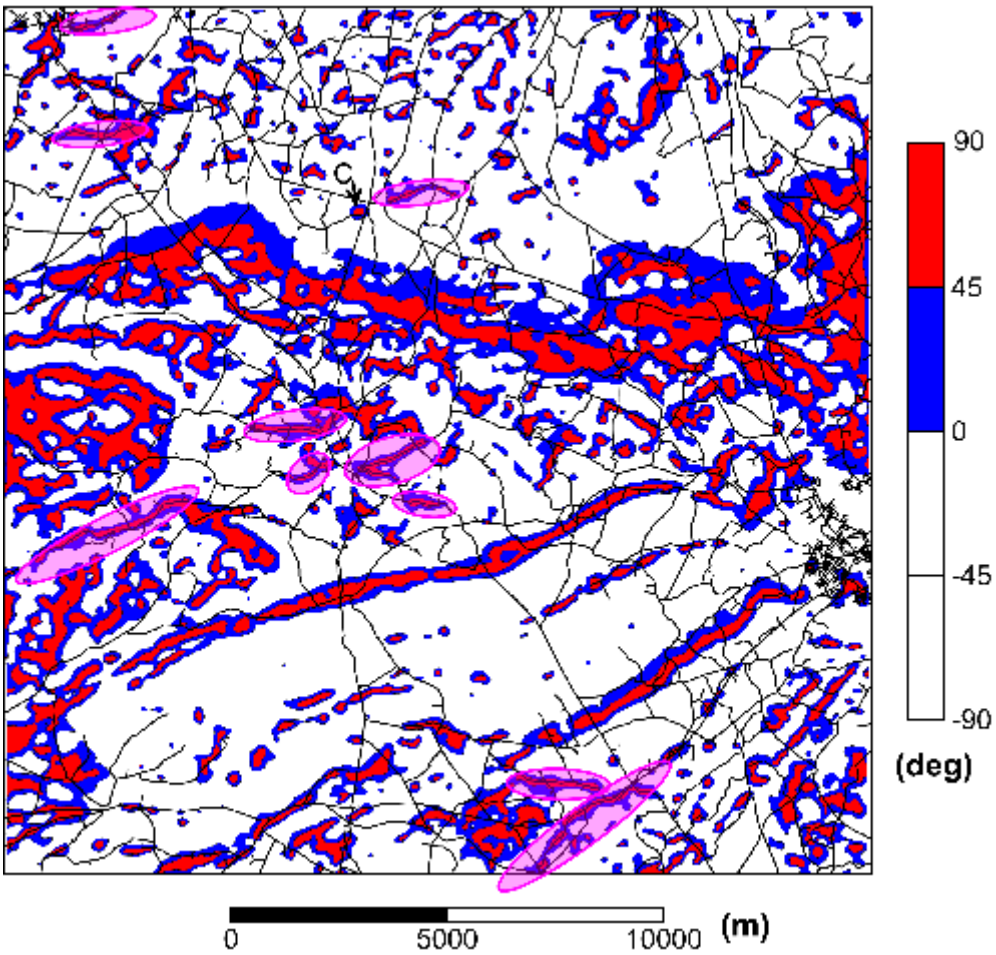

Figure 11. The tilt derivative (TDR) of the upward continued (100 m) conductivity data across the test area (20 x 20 km), same as shown in Figure 10. Background lines are from a database of the centre-lines of roads across the area. Letter C and arrow denotes a cultural perturbation discussed in the text. Ellipses with transparent infill indicate zones in which positive values of the TDR appear associated with roads.

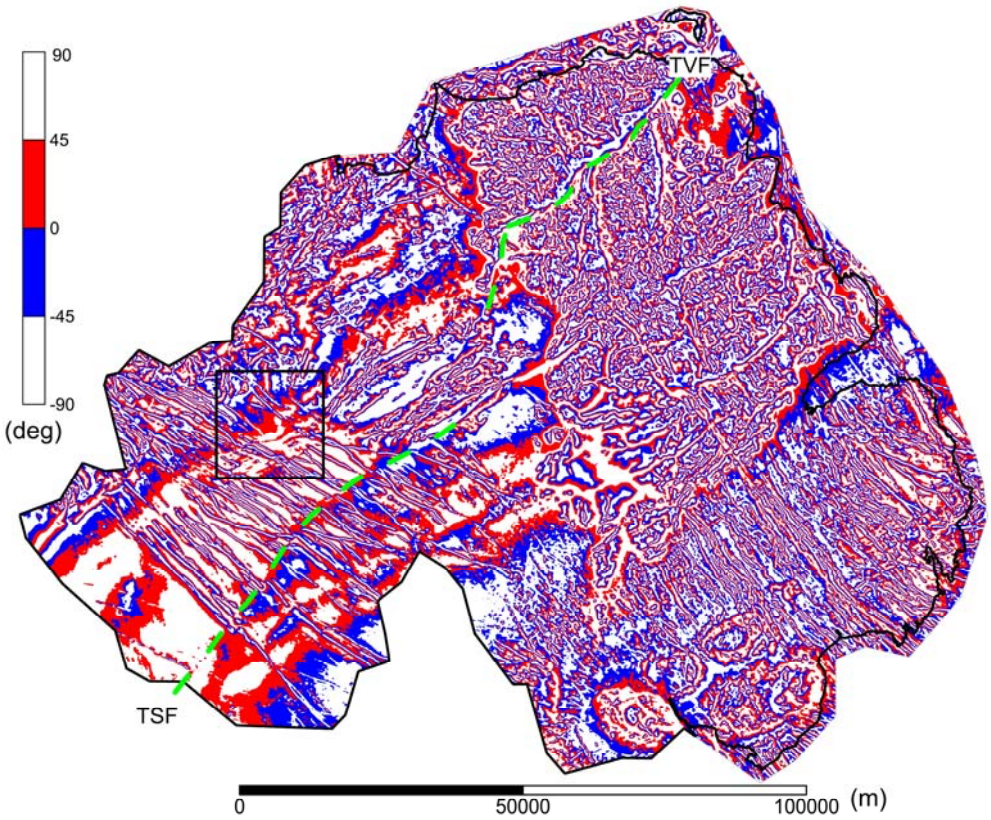

Figure 12. Tilt derivative (TDR) of the upward continued (200 m) magnetic data for the Tellus survey. TDR response contoured using an interval of 45º with only two intervals shown with infill. Location of 20 x 20 km test area shown as a rectangle. Location of two faults (TVF=Tow Valley Fault, TSF= Tempo-Sixmilecross Fault) shown with green dotted lines.

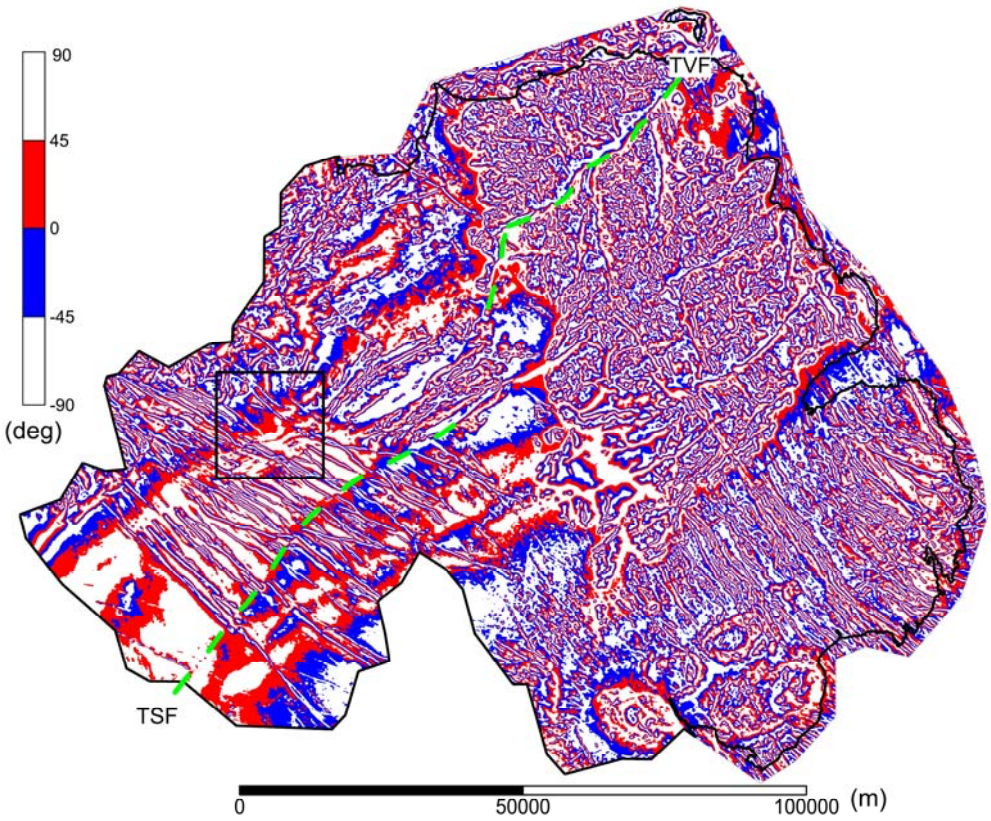

Figure 12. Tilt derivative (TDR) of the upward continued (200 m) magnetic data for the Tellus survey. TDR response contoured using an interval of 45º with only two intervals shown with infill. Location of 20 x 20 km test area shown as a rectangle. Location of two faults (TVF=Tow Valley Fault, TSF= Tempo-Sixmilecross Fault) shown with green dotted lines.

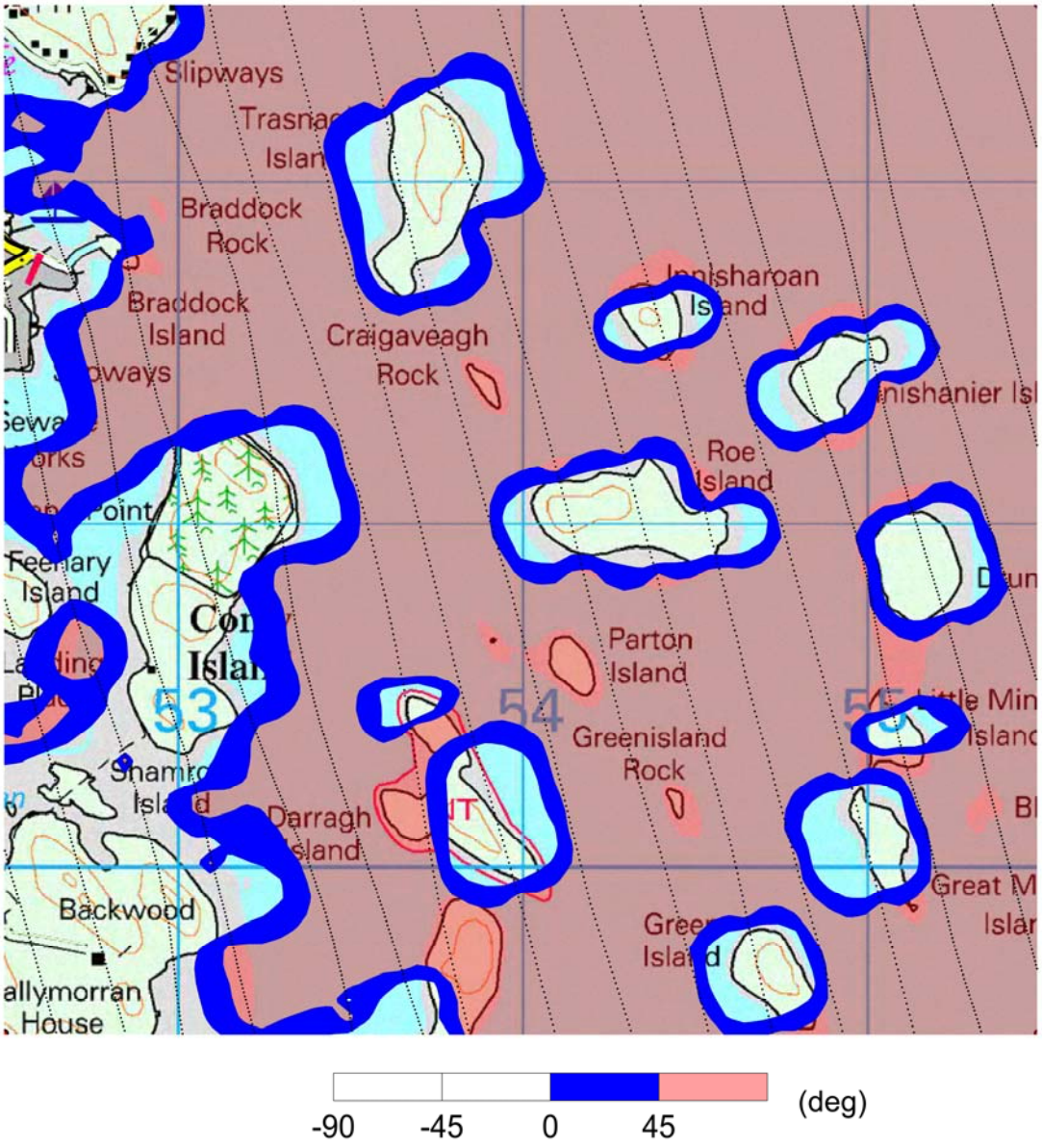

Figure 14. Tilt derivative (TDR) of the conductivity data across a 3 x 3 km test area (shown in Figure 13). Frequency is 3125 Hz and 200 m flight lines are shown as dots. TDR response contoured using an interval of 45º with only two intervals shown with infill. The infilled contour interval from 45º to 90º is transparent. The background is a 1:50k topographic map showing the western coast of Strangford Lough and a series of offshore islands/rocks. Map contains grid squares at a 1 km interval for scale.